Eco-Environment & Health 3 (2024) 89–106

Contents lists available at ScienceDirect

Eco-Environment & Health

journal homepage: www.journals.elsevier.com/eco-environment-and-health

Review

Understanding the role of manganese oxides in retaining harmful metals: Insights into oxidation and adsorption mechanisms at microstructure level

Feng Li [a,b,f], Hui Yin [c,d], Tianqiang Zhu [a,b,f], Wen Zhuang [a,b,e,f,*]

[a] School of Environmental Science and Engineering, Shandong University, Qingdao, Shandong 266237, China
[b] Institute of Marine Science and Technology, Shandong University, Qingdao 266237, China
[c] Key Laboratory of Arable Land Conservation (Middle and Lower Reaches of Yangtse River), Ministry of Agriculture and Rural Affairs, College of Resources and Environment, Huazhong Agricultural University, Wuhan 430070, China
[d] State Environmental Protection Key Laboratory of Soil Health and Green Remediation, Ministry of Ecology and Environment, Huazhong Agricultural University, Wuhan 430070, China
[e] National Laboratory for Marine Science and Technology, Qingdao 266237, China
[f] Institute of Eco-environmental Forensics, Shandong University, Qingdao 266237, China

ARTICLE INFO

Keywords:
Manganese oxides
Harmful metals
Adsorption
Redox
Environment

ABSTRACT

The increasing intensity of human activities has led to a critical environmental challenge: widespread metal pollution. Manganese (Mn) oxides have emerged as potentially natural scavengers that perform crucial functions in the biogeochemical cycling of metal elements. Prior reviews have focused on the synthesis, characterization, and adsorption kinetics of Mn oxides, along with the transformation pathways of specific layered Mn oxides. This review conducts a meticulous investigation of the molecular-level adsorption and oxidation mechanisms of Mn oxides on hazardous metals, including adsorption patterns, coordination, adsorption sites, and redox processes. We also provide a comprehensive discussion of both internal factors (surface area, crystallinity, octahedral vacancy content in Mn oxides, and reactant concentration) and external factors (pH, presence of doped or pre-adsorbed metal ions) affecting the adsorption/oxidation of metals by Mn oxides. Additionally, we identify existing gaps in understanding these mechanisms and suggest avenues for future research. Our goal is to enhance knowledge of Mn oxides' regulatory roles in metal element translocation and transformation at the microstructure level, offering a framework for developing effective metal adsorbents and pollution control strategies.

1. Introduction

Manganese (oxyhydr)oxides (hereafter referred to as Mn oxides) are minerals prevalent in both terrestrial and aquatic environments. Although they constitute only about 1 % of soils and sediments, Mn oxides often appear as fine particles, gelatinous aggregates, and spherical or massive nodules at the interfaces of lithosphere, hydrosphere, atmosphere, and biosphere. Through coating the surfaces of other minerals, Mn oxides demonstrate a potential activity that extends far beyond what their overall quantity would suggest [1–4].

The common valence states of Mn encompass II, III, and IV. Mn(II) and Mn(IV) exhibit great stability in natural environments, capable of transforming between soluble low-valence states and insoluble high-valence states [5–9]. Mn(III) is thermodynamically unstable, existing stably only in specific soluble organic complexes or minerals; it often disproportionates into Mn(II) and Mn(IV) [10,11]. Consequently, the genesis of Mn oxide solid phases in natural systems typically begins with Mn(II) species, which undergo a sequence of biological and abiotic oxidation processes, including microbial enzyme activity, reactive oxygen species, and mineral surface catalysis [12–16]. Initially, Mn oxides manifest as layered phases that are characterized by poor crystallization, high disorder, and high reactivity. Subsequently, these newly formed Mn oxides undergo diagenesis and transformation at oxygen-anoxic interfaces, like marine sediments, which give rise to reduction potential gradients within a few centimeters of the sediment and facilitate continuous redox cycles between Mn(II) and Mn(IV) [17,18]. Over 30 forms of natural Mn oxides, resulting from intricate biogeochemical processes, including precipitation, dissolution, maturation, and transformation, are found in contemporary environments [19]. The major Mn oxides commonly found in soil and water sedimentary environments are summarized in Table 1.

The basic unit of the crystal structure of Mn oxides includes an MnO_6 octahedron with an Mn atom located at the center and six oxygen atoms surrounding it. The MnO_6 octahedra connect via edge-sharing to form

* Corresponding author.
E-mail address: wzhuang@sdu.edu.cn (W. Zhuang).

https://doi.org/10.1016/j.eehl.2024.01.002
Received 7 September 2023; Accepted 8 January 2024
Available online 23 January 2024

Table 1
Common types of Mn oxide mineral in soils and sediments.

Structure type		Mineral	Category	Chemical formula	References
Layer structure		Birnessite	δ-MnO_2	$(Na,Ca,K)Mn_7O_{14}·2.8H_2O$	[20]
		Vernadite	δ-MnO_2	$MnO_2·nH_2O$	[21]
		Buserite		$(Ca,Na,K)_x$ $(Mn^{4+},Mn^{3+})O_4·nH_2O$	[22]
		Lithiophorite		$LiAl_2(Mn^{4+}{}_2,Mn^{3+})O_6·(OH)_6$	[23]
		Asbolane		$(Ni,Co)_xMn^{4+}(O,OH)_4·nH_2O$	[23]
Tunnel structure		Pyrolusite	β-MnO_2	MnO_2	[24]
		Ramsdellite	γ-MnO_2	MnO_2	[24,25]
		Nsutite	γ-MnO_2	$Mn(O,OH)_2$	[26]
		Hollandite	α-MnO_2	$Ba_x(Mn^{4+},Mn^{3+})_8O_{16}$	[27]
		Cryptomelane	α-MnO_2	$K_x(Mn^{4+},Mn^{3+})_8O_{16}$	[27]
		Manjiroite		$Na_x(Mn^{4+},Mn^{3+})_8O_{16}$	[28]
		Coronadite	α-MnO_2	$Pb_x(Mn^{4+},Mn^{3+})_8O_{16}$	[17]
		Romanechite		$(Ba,K,Mn^{2+})Mn_5O_{10}·xH_2O$	[28]
		Todorokite		$(Ca,Na,K)_x(Mn^{4+},Mn^{3+})_6O_{12}·3.5H_2O$	[29]
Low-valence Mn oxide mineral	Tunnel structure	Manganite	γ-MnOOH	MnOOH	[30]
		Feiknechite	β-MnOOH	MnOOH	[17]
		Groutite	α-MnOOH	MnOOH	[30]
	Other Mn minerals	Hausmannite		$Mn^{2+}Mn^{3+}{}_2O_4$	[31]
		Manganosite		MnO	[2]
		Bixbyite		Mn_2O_3	[32]

single chains, producing Mn oxides with diverse structures through edge- and/or corner-sharing [33]. Based on the stacking arrangement of MnO_6 octahedra, the Mn oxides are typically classified into two categories: layered structure (i.e., phyllomanganate) and tunneled structure (i.e., tectomanganate) [34–36]. The layered structure comprises layers of edge-sharing MnO_6 octahedra, with symmetry dependent on the Mn(III) octahedra distribution. The tunneled structure, however, involves edge-sharing MnO_6 octahedra forming tunnel walls or floor/ceiling [35]. Heterovalent Mn ions and/or foreign transition metal cations may be present in both layered and tunnel-structured Mn oxides, either replacing Mn(IV) structurally or acting as charge compensators in phyllomanganate interlayers or tectomanganate tunnels [37–40]. Common examples include birnessite, buserite, and vernadite for layered Mn oxides; pyrolusite (β-MnO_2), manganite (γ-MnOOH), cryptomelane, and todorokite for tunneled Mn oxides [41]. These distinct Mn oxide layers and tunnels exhibit varying sizes and crystal structures and thus exhibit different redox, adsorption, electrochemical, and photochemical reactivity [41].

For a long time, the contamination of soil and wastewater by harmful metals, particularly heavy metals, has emerged as a major environmental issue due to increased human activities such as mining, metal industries, incinerators, power plants, and agricultural use of sewage sludge, insecticides, and fertilizers [42,43]. Natural Mn oxides, with their low point of zero charge (PZC), large surface area, high negative charge, and high reduction potential, are key in controlling harmful metal concentrations, especially heavy metals, through adsorption, coprecipitation, and redox reactions [2,5,18,44–51]. Compared to traditional adsorbents like aluminum (Al) oxides, iron (Fe) oxides, green clay polymer sulfur, and carbon-based materials, Mn oxides offer superior adsorption efficiency and stability for metal removal from water [52–56]. They exhibit greater adsorption capacities for toxic metals like copper (Cu), cobalt (Co), nickel (Ni), zinc (Zn), lead (Pb), and cadmium (Cd) than Al oxides and Fe oxides [57–59]. Mn oxides also possess the advantages of being cost-effective, minimally toxic, environmentally friendly, and easily manageable compared to synthetic adsorbents [60–64]. Additionally, Mn oxides serve as natural oxidants for variable valence metals such as arsenic (As), Co, chromium (Cr), selenium (Se), thallium (Tl), and vanadium (V) [57,65–67]. The high redox potential of Mn oxides, evidenced by the standard electrode potential (1.23 eV) of $MnO_2 + H^+/Mn^{2+}$, (>1.3 eV) of Mn^{3+}/Mn^{2+}, is comparable to or higher than that of $O_2 + H^+/H_2O$ (1.229 eV) [68]. This property enables Mn oxides to alter the valence, chemical form, and thus bioavailability of harmful metals through oxidation [69,70]. The adsorption and oxidation effectiveness of Mn oxides can be further enhanced through electrochemical regulation of the degree of redox [71–73].

In recent decades, extensive research has significantly enhanced our understanding of the formation, structure, and metal adsorption/oxidation mechanisms of Mn oxides, with ongoing studies providing fresh perspectives. This review aims to consolidate current knowledge in the field, covering: (1) common types of Mn oxides and their structural characteristics in the natural environments; (2) the adsorption/oxidation mechanisms of metals, including alkali and transition metals, on Mn oxides; (3) key factors influencing metal adsorption and oxidation by Mn oxides, including mineral crystallinity, surface area, reactant concentration, pH, Mn valence, octahedral vacancies, and competitive metal ions. Furthermore, the review suggests directions for future research. The ultimate objective is to deepen understanding of Mn oxides' regulatory role in the environmental mobility and transformation of metal elements and to provide a framework for developing effective metal adsorbents and pollution control strategies.

2. Common Mn oxides in natural environments

Layered and tunneled Mn oxides are ubiquitous Mn oxide minerals found in both terrestrial and aquatic environments [18,37,74]. The transformation of layered Mn oxides into tunneled Mn oxides can occur under specific physicochemical or biological conditions [18,75].

2.1. Layered Mn oxides

2.1.1. Birnessite

Birnessite is a prevalent Mn oxide found in various environments. It is composed of stacked layers along the c^* axis resulting from the stacking and interaction of a layer of MnO_6 octahedra with shared edges and an interlayer containing water and alkaline/alkaline earth metals (Fig. 1) [16,20,59,76,77]. Charge defects in birnessite layers arise from vacancies, the substitution of layer Mn^{4+} with lower valence cations like Mn^{3+}, Ni^{2+}, and Co^{3+}, and edge sites [35,78]. The defects can be neutralized by Mn^{3+}, Mn^{2+}, H^+, interlayer alkaline/alkaline earth metals, and other cations [79,80]. By varying the interlayer metal species, different birnessite subtypes emerge: Na-birnessite, Mg-birnessite, and K-birnessite correspond to Na^+, Mg^{2+}, and K^+ in the interlayer, respectively [81]. When the interlayers contain hydrated Ca^{2+} or Mn^{2+}, the minerals are termed ranceite and takanelite, respectively. In the presence of large cations such as Ca^{2+}, Mg^{2+}, Ni^{2+}, Co^{3+}, and La^{3+}, the interlayer spacing expands from 0.7 nm to 1 nm. Additionally, these Mn

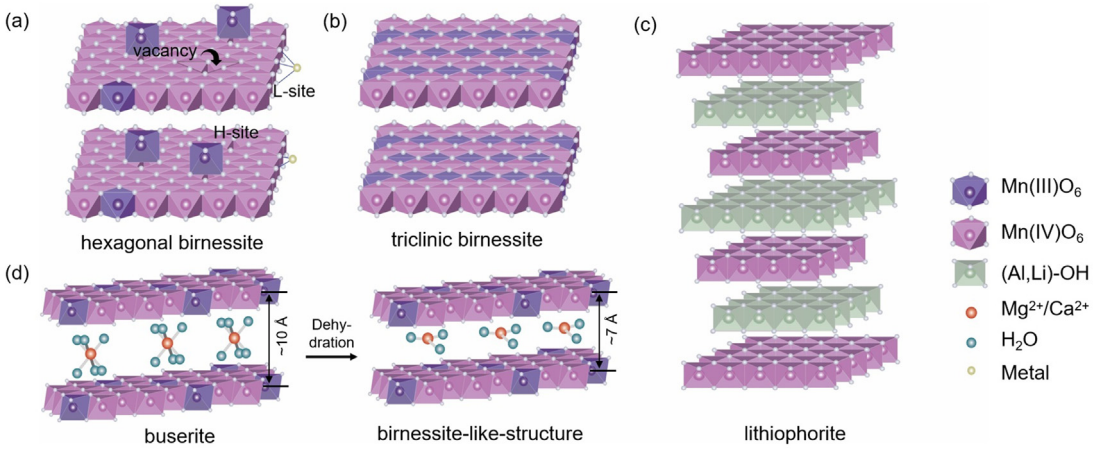

Fig. 1. Structural illustrations of common layered manganese oxides. (**a**) Hexagonal birnessite. H-site represents octahedral vacancy sites; L-site represents particle edge sites. (**b**) Triclinic birnessite. (**c**) Lithiophorite. (**d**) The transformation pathway of buserite. (d) is adapted with permission from the study by Lee and Xu [22]. Copyright 2016, Clay Minerals Society.

oxides presented a poor crystallinity in nature, lacking a fixed stoichiometric composition [82].

Birnessite samples are generally classified into two groups based on the symmetry of the [MnO_6] layer: hexagonal and triclinic. It is proposed that the inclusion of cell symmetry can serve as a supplement to the current mineral nomenclature and the subdivision of birnessites into hexagonal and triclinic crystal systems [16]. The fundamental distinction between these types lies in the origin of charge defects, nature of interlayer cations, and oxidation states of layer and/or interlayer Mn [83]. Hexagonal birnessites contain octahedral layers of Mn(IV)O_6 and/or Mn(III)O_6, with octahedral vacancies [84]. These vacancies result in a layer with negative charges, balanced by interlayer H^+ and/or interlayer $Mn^{3+/2+}$ positioned above or below the vacancies [84,85]. In contrast, triclinic birnessite features octahedral layers with an alternating sequence of two Mn(IV)O_6 rows and one Mn(III)O_6 row along the *b*-axis, and lacks octahedral vacancies [86]. The substitution of some Mn(IV) with Mn(III) in the MnO_6 octahedron results in charge deficiency in the layer [87,88], which is compensated by cations associated with water molecules (typically K^+ or Na^+) in the interlayer space [89].

Laboratory synthesis of analogs to natural birnessites is achievable. Depending on synthesis approaches, the resulting birnessites are categorized as either acidic or alkaline [90], each exhibiting distinct structural features and Mn content in various valence states. Acid birnessites, synthesized in a low pH medium, belong to the hexagonal crystal system [16,91]. These birnessites possess numerous octahedral vacancies (up to 12 %) in the layers, primarily composed of Mn(IV) with a smaller amount of Mn(III), while the interlayer ions consist mainly of H^+, Mn^{3+}, and Mn^{2+} [33,84]. Alkaline birnessites are typically created by fully oxidizing $Mn(OH)_2$ with $KMnO_4$ in a weakly alkaline medium, and triclinic birnessites are generally synthesized in alkaline conditions [92–94]. Alkaline birnessites have a higher Mn(III) content in their layers than acidic birnessites, and their interlayers consist of Mn^{3+} and Mn^{2+}, with fewer H^+ [84].

2.1.2. Vernadite

Vernadites are characterized by a layered arrangement of MnO_6 octahedra, connected by edge-sharing, and typically feature nanocrystalline particles in natural samples [21,95]. Chemical properties and X-ray diffraction (XRD) data have identified three distinct types of vernadites: the ~7 Å type, the ~10 Å type, and the Fe type [37,96]. The ~7 Å and ~10 Å types are distinguished by the presence of one or two layers of water molecules in the interlayer, whereas the Fe-type vernadites have a unique monolayer structure [37,84]. Their XRD patterns have distinct diffraction peaks at 2.42–2.43 Å, 1.41 Å, and 1.22 Å, respectively. The *d*-spacing ratio of the first two strong diffraction peaks (1.72) closely aligns with the value of $3^{1/2}$, indicating the pseudo hexagonal symmetry of the Mn octahedral layer. Furthermore, the near-symmetrical shape of the 1.41 Å peak indicates a correlation between the layered structure and hexagonal symmetry [97].

Vernadite structures are often distorted due to vacancies and substitution of layer Mn by other cations like Ni^{2+}, Cu^{2+}, Mn^{3+}, and Fe^{3+} [97–99]. As vernadites are characterized by low crystallinity, high-density defects, and predominantly mixed phases, their structures remain incompletely elucidated [97]. They possess extensive edge-specific surface areas, resulting in a relatively high ratio of edge sites to total sites, which significantly enhances their capacity for metal ion adsorption at edge sites [100]. Additionally, vernadites exhibit significant amphoteric reaction sites due to their extensive edge-specific surface areas [100].

2.1.3. Buserite

Buserite is a type of Mn oxide mineral that is characterized by its layered structure, consisting of two layers of water molecules located within the interlayer region (Fig. 1) [22,101]. Typically, the metal ions in the interlayer area of buserite are bound to water molecules, similar to those in birnessite and vernadite [102,103]. Na-buserite is a common type of buserite, which exhibits the strongest diffraction peaks at 10.1–10.2 Å and 5.0–5.1 Å [22].

The stability of buserite's structure largely depends on the hydration enthalpy of interlayer ions. High interlayer cation content in buserite minerals makes them more resistant to conversion into birnessite. Conversely, birnessite can be converted into buserite upon the inclusion of specific cations like Mg^{2+}, Ca^{2+}, and Ni^{2+} [22,104]. Moreover, hydrothermal processing of buserite can lead to the production of todorokite. The synthetic methods for todorokites mainly differ in the initial synthesis of layered Mn oxides and the specific metal ions incorporated into the interlayer of the precursor, resulting in Me-buserite (where “Me” typically represents Mg ions) [105,106]. Cui et al. [105] showed that reflux treatment in the atmosphere of Na-buserite could facilitate its conversion into todorokite, indicating the effectiveness of aging treatments in this transformation process.

2.1.4. Asbolane and lithiophorite

Asbolane and lithiophorite exhibit comparable hexagonal symmetry and layered structure with metal (hydrogen) oxide interlayers (Fig. 1) [107]. However, the asbolane features an island-like structure formed by Ni/Co (hydrogen) oxides in the interlayers [108], whereas the lithiophorite features Li and Al hydroxide interlayers (Fig. 1). Despite these structural differences, they share similar optical properties [23,109].

Asbolane, a Mn(IV) hydroxide exhibiting a higher oxidation state, lacks a constant molecular formula [110]. Lithiophorite has been categorized as the third type of Mn oxide, alongside layered and tunnel structures, due to its mixed layer structure [111]. Lithiophorite discovered in soil exhibits good crystallinity, a small specific surface area, and a slow weathering rate [111]. Asbolane and lithiophorite frequently coexist in the environment, leading some scholars to posit that asbolane is a variant of lithiophorite in which interlayer aluminum is substituted by transition metals [108]. Burlet and Vanbrabant [23] have proposed that the intermediate phase between asbolane and lithiophorite is the asbolane–lithiophorite intermediate. The primary distinction among them is differentiated by varying concentrations of Co, Ni, Cu, and Li in their oxides.

2.2. Tunneled Mn oxides

Tunnel-structured Mn oxides consist of MnO_6 octahedra chains that share edges and corners with neighboring chains, arranged in an m × n rectangular configuration. The size of the tunnels, defined by the number of chains, accommodates large cations (e.g., Mg^{2+}, Ca^{2+}, Ba^{2+}, Na^{+}, K^{+}) and water molecules [112–115]. Commonly found tunnel-structured Mn oxide minerals in nature include pyrolusite (1 × 1 configuration), Ramsdellite (1 × 2), nsutite (mixture of 1 × 1 and 1 × 2), cryptomelan (2 × 2), romanechite (2 × 3), and todorokite (3 × 3), with the rare occurrence of woodruffite (3 × 4) [116–122]. Under specific conditions in soil or sediments, layered Mn oxides can undergo a transformation into tunnel-structured Mn oxides [18,37,102,103,123].

2.2.1. Todorokite

Todorokite, a prominent Mn mineral found in marine ferromanganese nodules and crusts [37,124–126], is characterized by its tunnel structure composed of triple chains of edge-sharing Mn(IV)O_6 octahedra that are corner-shared with adjacent triple octahedral chains. This arrangement results in a 3 × 3 tunnel structure, providing a significant tunnel cavity per unit cell measuring 6.9 × 6.9 Å [29,123,127,128]. The tunnels present in natural samples exhibit a partial occupancy of water molecules and a diverse range of cations, such as Mg^{2+}, Ca^{2+}, K^{+}, Na^{+}, and Ba^{2+} [124,127]. Moreover, todorokite holds promising economic significance due to its frequent association with strategically important metals such as Co^{2+}, Ni^{2+}, Cu^{2+}, and platinum group metals, as well as rare earth elements [37].

In natural occurrences, todorokite often exhibits poor crystallinity and is commonly found in combination with other poorly crystalline oxyhydroxides like vernadite [129,130]. The formation of todorokite is generally believed to stem from layer-structured Mn oxides with triclinic symmetry. Traditionally, the conversion of birnessite to todorokite is explained as a topotactic process, wherein certain morphological characteristics and structural components of the initial phyllomanganate are retained in the newly formed todorokite [34,102,130,131]. Atkins et al. [102] proposed a four-stage mechanism for this conversion. Furthermore, recent research also indicates that todorokite predominantly occurs in deeply buried nodules, suggesting that phyllomanganates can transform into todorokite under relatively suboxic conditions as well [126,132].

Todorokite, a prevalent tectomanganate mineral, plays a crucial role in the biogeochemical cycling of trace metals. Although its external edge surfaces possess a considerably smaller surface area than its intra-tunnels, metal diffusion occurs more rapidly along the external surface than within the tunnels [127,133,134]. Kim et al. [135] proposed a surface-loading-dependent mechanism, characterized by high affinity, which plays a dominant role during the initial adsorption stage. Conversely, the intra-tunnel sites act as slow sites, significantly responsible for the overall cation adsorption capacity.

2.2.2. Pyrolusite

Pyrolusite, a tunnel-structured Mn oxide, exhibits a high degree of crystallinity. The MnO_6 octahedron in pyrolusite is arranged in a single chain with an edge connection, with adjacent chains sharing corners to create a 1 × 1 tunnel structure (Fig. 2). The small size of the tunnel structure in pyrolusite makes it difficult to accommodate additional ions or water molecules [24,136,137]. The structure of pyrolusite and manganite can transform under specific conditions [138]. Manganite represents a distorted form of pyrolusite, arising from partial substitution of Mn(IV) by Mn(III) in pyrolusite, and subsequent charge compensation by H^{+}. This process leads to a reduction in symmetry from the tetragonal system to the orthorhombic system. Upon oxidation, manganite can be transformed into pyrolusite [30].

2.2.3. Ramsdellite

The ramsdellite possesses a tunnel structure of 1 × 2, where Mn(IV)O_6 octahedrons are linked into double chains. Each double chain is composed of two adjacent single chains that share the edge of the octahedrons (Fig. 2). The crystal structure of ramsdellite is akin to pyrolusite, with the exception that the single chain of pyrolusite octahedron is substituted by the double chain in ramsdellite. The double chains are corner-connected to form a framework, creating a rectangular cross-sectional tunnels [24,136]. Ramsdellite is commonly found in localized oxidation areas of Mn-rich sediments and is considered a metastable MnO_2 [139].

Ramsdellite exhibits isomorphism with minerals such as goethite (FeOOH), gibbsite (AlOOH), and groutite (MnOOH). Under specific conditions, ramsdellite and groutite can undergo an interconvert [30]. Groutite exhibits the formation of strong hydrogen bonds through OH groups. While ramsdellite is ostensibly devoid of hydrogen, certain ramsdellite samples display weak hydrogen bonds formed by OH groups [140].

2.2.4. Nsutite

Nsutite, a Mn oxide mineral with a higher water content [118], is widely distributed and possesses a 1 × 1 and 1 × 2 tunnel structure (Fig. 2) [141]. Its XRD diffraction pattern is similar to that of ramsdellite, categorizing it as a distinct form of γ-MnO_2 [139]. Some nsutite samples exhibit tunnel structures larger than the typical 1 × 1 (pyrolusite) and 1 × 2 (ramsdellite), such as 1 × 3 and 3 × 3 tunnels, as well as various defects and grain boundaries [142]. The tunnel configuration of nsutite typically includes trace amounts of ions such as Na^{+}, Ca^{2+}, Mg^{2+}, K^{+}, Zn^{2+}, Ni^{2+}, Fe^{3+}, Al^{3+}, Si^{4+}, along approximately 2%–4% water (w/w). These constituents may be accommodated within larger tunnels or along grain boundaries. Charge balance is maintained by partially substituting Mn(IV) with Mn(III) [2].

Nsutite is a secondary substitute mineral that typically arises from the oxidation of Mn carbonate minerals [118]. Another type of manganoan nsutite exhibits poor structural stability due to its high water content and low-valence Mn(III)/Mn(II) with a large ionic radius. Upon heating, manganoan nsutite can transform into standard nsutite [118].

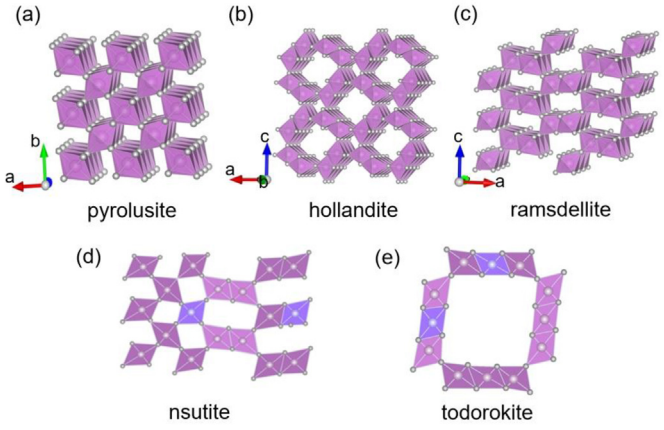

Fig. 2. Common tunneled Mn oxides. Mn, manganese.

2.2.5. Hollandite

The α-MnO_2 mineral, known as hollandite, features a 2 × 2 tunnel structure similar to ramsdellite. This structure is comprised of double chains of edge-sharing MnO_6 octahedra, forming a tunnel with square cross sections (measuring two octahedra on a side of 4.6 Å × 4.6 Å) (Fig. 2). The tunnel cavities typically host large monovalent or divalent cations, in some cases, water molecules [2,119]. The metal ions (Me^{n+}) within the tunnels are commonly understood to bond with oxygen atoms in the structure, with each Me–O bond exhibiting an equal distance. The tunnel center can be occupied by various Me^{n+}, including Ba^{2+} (in hollandite), K^+ (in cryptomelane), Pb^{2+} (in coronadite), and Na^+ (in manjiroite) [27,143–145]. The inclusion of Me^{n+} within the tunnel has the potential to reinforce the structural integrity of the tunnel and prevent collapse [27]. The tunnel's chemical composition exhibits a notable degree of adaptability, stemming not only from cation exchange within the tunnel but also from the replacement of the octahedral framework [115]. This adaptability contributes to the versatility of hollandite in various environmental and geological contexts.

3. The adsorption and oxidation mechanisms of harmful metals by Mn oxides

3.1. Adsorption

Both layered and tunneled Mn oxides play significant roles in metal adsorption, but they exhibit notable differences in their adsorption capacities. In layered Mn oxides, interlayer cations form strong inner-sphere surface complexes at the vacancy sites. Conversely, tunneled Mn oxides feature a combination of inner-sphere complexes at the tunnel corner sites and outer-sphere complexes coordinated with six water molecules at the tunnel center sites [127,133]. Previous research has demonstrated that birnessite exhibits a greater capacity for adsorbing metal ions than todorokite [146]. Consequently, layered Mn oxides, particularly birnessites, are more prevalent and effective in the geological milieu [147–149].

The accumulation of heavy metals and transition metal elements in Mn oxides is attributed to the obligate and selective adsorption processes, closely related to the properties of the adsorbed ions and the surface properties of Mn oxides [51]. The oxygen component of Mn oxides can be classified into two distinct chemical states, namely, saturated oxygen and unsaturated oxygen, with the latter constituting approximately 20% of the surface area and serving as crucial adsorption sites [150]. The structure of birnessite includes two main types of allosteric sites, namely octahedral vacancy sites (H-site) in layers and particle edge sites (L-site) (Fig. 1). In some minerals, a low-energy site (L-II site) exists, characterized by its tridentate arrangement and proximity to octahedral vacancies. For these sites to be effective, the vicinity of interlayer Mn(III) is essential. The presence of Mn(III) results in the formation of additional unsaturated oxygen within the layer, thereby rendering low-energy sites within the layer [151].

Heavy metals and transition metals, with their high nuclear charges, small ionic radii, strong polarization and deformation capabilities, are easy hydrolysis to form hydroxylated cations and exhibit specific and selective adsorption on Mn oxide surfaces by forming stable inner-sphere complexes [51]. The adsorption mechanisms of layered Mn oxides, especially birnessites, for transition metals can be succinctly delineated as follows: (1) metal ions engage in intricate reactions with surface hydroxyl groups, resulting in the formation of hydroxyl complexes that are linked by coordination bonds. The strength of adsorption directly correlates to the stability constants or hydrolysis constants of the hydroxylated cations [51,147,152,153]; (2) metal ions participate in an exchange process with surface Mn(II) to produce highly stable inner-sphere complexes [48,129,151,154,155]; (3) transition metal cations preferentially adsorb above or below octahedral vacancies in birnessites, or integrate into vacancies, becoming part of the hexagonal layers (Fig. 3) [35,78,150,156–158]. Additionally, metal cations can adsorb at the edge sites of the layer structure through double-corner-sharing (DCS) or double-edge-sharing (DES) (Fig. 3) [100,159]. The octahedral vacancies within the layer are preferred sites for cation adsorption, whereas layer edges are exclusive for anion adsorption [160].

During Me^{2+} adsorption, the simultaneous release of Na^+, H^+, and K^+ into the solution occurs, and the quantities of released Na^+, H^+, and K^+ exhibit a linear increase in relation to Me^{2+} adsorption. Therefore, the determination of metal adsorption can be inferred from the quantities of Na^+ and K^+ released [95,161]. Simultaneously, the content of Na^+ or K^+ influences the structure of Mn oxides. For instance, decreasing K^+ concentrations in birnessite interlayers significantly diminishes the hydrogen bonding, reducing the stabilization of MnO_6 layers connected by K^+ ions between adjacent layers. This reduction in hydrogen bonding may explain the observed decrease in MnO_2 sheet stacking in these birnessites [162,163]. The promotion of the conversion of c-axis disordered birnessite to todorokite is facilitated by the presence of Na^+, as evidenced by various studies [79,81,89,164,165]. Conversely, interlayer K^+ appears to have an opposing effect. The contraction or expansion of the (001) basal spacing of Na-birnessite is contingent upon the ratio of exchanged K^+ and the content of interlayer water [81,89]. Therefore, Na^+ and K^+ ion exchanges induce structural alterations in Mn oxides, consequently impacting their metal adsorption capabilities.

The metal adsorption capacity of Mn oxides can be enhanced through the electrochemical methods [166–170]. For instance, during a charge–discharge process in a Zn^{2+}-containing solution, Zn^{2+} ions are adsorbed at the vacancies of birnessite and inserted into the interlayer, leading to the transformation of birnessite into zinc-buserite and hetaerolite [166]. Previous investigations have demonstrated that birnessite can effectively remove Cu^{2+} through multiple cycles of electrochemical redox reactions. These reactions alter the chemical composition and initiate a dissolution–recrystallization process, which increases the interaction between birnessite and heavy metal ions, exposing more active sites on the electrode for electrosorption [167]. In the case of cadmium adsorption, Cd^{2+} ions are adsorbed onto the surfaces and interlayers of birnessite, with the recrystallization process expanding the effective adsorption area, consequently augmenting the metal adsorption capacity. The maximum electrosorption capacity of birnessite for Cd^{2+} ions was determined to be approximately 900.7 mg/g, which is significantly greater than its adsorption isotherm capacity (125.8 mg/g) [168]. This demonstrates the potential of electrochemical methods in boosting the metal adsorption capabilities of Mn oxides.

3.2. Oxidation

Mn oxides are among the most potent oxidizing solids in Earth's surface environments [171,172]. These oxides, particularly known for their oxidizing properties, include layered structures like birnessite, vernadite, and buserite with a hexagonal structure, alongside certain tunnel Mn oxides such as pyrolusite and todorokite [69,127]. The Mn(IV)/Mn(II) redox pair, with its high redox potential, is effective in oxidizing a wide range of metals, including but not limited to Cr, U, As, Se, Tc, Np, Pu, Co, Sb, TI, and V [5,59,70,159,173].

The metal oxidation process on Mn oxides is believed to involve the adsorption of low-valent metal ions onto Mn oxides, followed by electron transfer [173,174]. The ratio of Mn(IV) in the mineral can influence its redox reactivity [175]. Furthermore, the redox ability of Mn oxide particles is influenced by several crucial factors, including the crystallinity of the particles, the Mn valence, the number of octahedral vacancies, and the presence of single and double coordinated oxygen atoms at the edge sites [85,159,174,176–178].

The redox reaction between metals and Mn oxides involves three fundamental stages: (1) metal ions adsorb onto the edge or interlayer of Mn oxides to create coordination complexes, either inner or outer-sphere coordination; (2) electron transfer takes place; (3) the coordination complexes dissociate [179]. Among these stages, the slowest process,

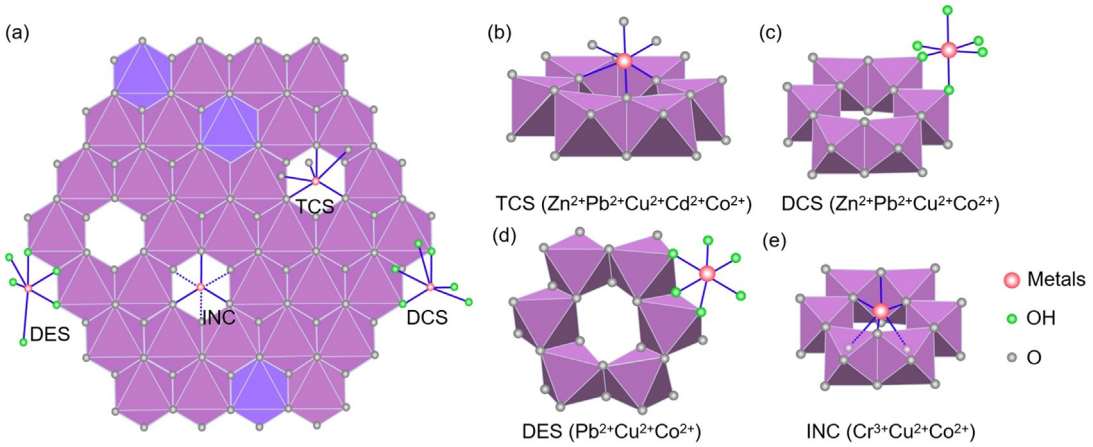

Fig. 3. Crystal structure of hexagonal birnessite (**a**) and possible surface complexation species of metals on birnessite **(b–e)**. (b) TCS, triple-corner-sharing complex; (c) DCS, double-corner-sharing complex; (d) DES, double-edge-sharing complex; (e) INC, incorporated inside a Mn vacancy. (a) is adapted with permission from ref. [44]. Copyright 2020, Elsevier.

often the electron transfer, typically acts as the rate-limiting step. In cases where the inner-sphere complex is formed, and the rate of coordination exchange of the reactant is slow, the formation of the coordination complex becomes the limiting step. However, if either or both of the reaction products are susceptible to coordination exchange, step (3) cannot be the limiting step [180]. For example, the oxidation of As(III) was initially believed to involve two separate electron transfer steps [181]. Recent studies suggest, however, that Mn(IV) undergoes direct reduction to Mn(II) upon receiving two electrons, without the generation of Mn(III) intermediate species, indicating a two-electron, single-step process [159,174]. In the case of Cr(III) oxidation, it is hypothesized that the reduction dissolution of Mn(IV) in birnessite occurs via two separate single-electron reactions, with the availability of Mn(III) significantly influencing the rate of Cr(III) oxidation [182].

Experimental investigations have demonstrated that during the reactions involving Mn oxides and metal reduction, oxidation transpires expeditiously at the outset, but subsequently decelerates until reaching a state of equilibrium. This trend indicates a gradual decrease in Mn oxides' reactivity, often ascribed to the mineral surface passivation [159,162,174,183,184]. Typically, surface passivation of Mn oxides is attributed to the accumulation of reaction products [185], especially Mn(II) generated by the reduction of Mn(IV), and metal ions adsorbed via oxidation [173]. Cationic agents are capable of passivating birnessite minerals, and in some cases, anionic agents are also capable of doing so [5,173,186]. The net positive charge on the edge sites of birnessite particles, especially evident at pH 4, due to proton adsorption, is attributed to the PZC of these sites [6,7]. Consequently, these positively charged edge sites have the ability to attract cationic agents, leading to passivation due to the accumulation of a substantial quantity of negative charges [78,186].

3.3. Typical harmful metals

To provide a detailed analysis of the adsorption and oxidation mechanisms of metals on Mn oxides, a considered selection of representative metal elements was undertaken. The selection criteria prioritized their capacity to accurately exemplify the mechanisms, rather than their potential harm to organisms. Detailed summaries of the interactions between Mn oxides and these selected metals are provided in the Supplementary Information (Table S1).

3.3.1. Lead

Birnessites exhibit the highest adsorption affinity and capacity for Pb^{2+} among common metal ions [147]. The structures of the complexes formed by Pb^{2+} at the vacancies and edge sites have been investigated using extended X-ray absorption fine structure (EXAFS) and density functional theory (DFT). These complexes include (1) triple-corner-sharing (TCS), where a Pb atom and three oxygen atoms (O_{II}) bind above/below the octahedral vacancies of the layer structure [153,154,157]; (2) TES, where Pb binds with two O_{II} and one surface O atom (O_{III}), and the O_{III} coordinates with Mn tridentate vacancies formed by the triangular shared Mn octahedron [156]; (3) DES, involving the bonding of a Pb atom to two singly and one doubly coordinated oxygen atoms at the layer edge [187]; (4) DCS, characterized by the bonding of a Pb atom to two adjacent MnO_6 octahedra on layer edge sites, with two single coordinated O atoms (Fig. 3) [154,156,188].

High-energy sites on birnessite surfaces, particularly those with vacancies, attract Pb^{2+} ions preferentially during surface interactions [20,153], followed by occupation of low-energy edge sites [151]. As a result, TCS surface complexes are formed above or below the vacancies at low surface Pb^{2+} loading. Under conditions of high Pb^{2+} loading, the formation of TES complexes occurs in close proximity to vacancies, as well as DCS and DES surface complexes along the edges [189,190]. As Pb load increases, Pb^{2+} coordination becomes distorted, resulting in significant distortion of the ideal Pb^{2+} coordination geometry and a notable decrease in coordination number. The instability of Pb-DCS depends on local coordination and hydration, with Pb-DES the primary remaining the primary edge surface species [187]. The higher density of internal vacancies compared to external vacancies results in greater adsorption of Pb^{2+} onto layer surfaces as TCS complexes [177].

Pb^{2+} adsorption onto birnessite is intricately associated with vacancies or substructures. Typically, Pb^{2+} can be adsorbed onto vacancies and edge sites. The proportions of Pb adsorbed on vacancies and edge sites are dependent on the particle size [191]. In contrast, other cations are proposed to be adsorbed onto vacancies. Pb^{2+}sorption capacity significantly surpasses that of most other heavy metals on birnessite [62], making Pb^{2+} a useful indicator for assessing vacancy content.

3.3.2. Zinc

Layered Mn oxides, specifically birnessite, predominantly adsorb Zn^{2+} at the octahedral vacancies, with the coordination geometry of Zn depending on the Zn loading, pH, and so on [156,157,172,192,193]. Grangeon et al. [192] reported that at low surface loadings, Zn^{2+} was primarily adsorbed in tetrahedral coordination (^{IV}Zn) as a TCS complex at vacancies. At higher loadings, both tetrahedral and octahedral (^{VI}Zn) coordinations coexist in the birnessite's structure. Kwon et al. [194] suggested that the ratio of ^{IV}Zn to ^{VI}Zn significantly influences the structural stability of birnessite.

Synchrotron micro-X-ray fluorescence spectroscopy (μ-SXRF), μ-XRD, and μ-extended X-ray absorption fine structure (μ-EXAFS) analyses

revealed that two-thirds of the Zn adsorbed by the octahedral vacancies of birnessite in soil iron-manganese nodules exist in the form of tetrahedral coordination, while the remaining one-third exists in the form of octahedral coordination [195]. The incorporation of Zn^{2+} into the structure results in the replacement of interlayer Na^{+} and Mn(III). At pH values of 6 or 8, DCS complexes are formed at the layer edges in addition to the TCS octahedral complexes at the vacancies (Fig. 3) [193].

3.3.3. Copper

The binding of Cu by layered Mn oxides occurs via three mechanisms, namely adsorption on octahedral vacancies, incorporation into the Mn layers, and adsorption at edge sites. Cu^{2+} adsorption onto vacancies entails the coordination with three surface oxygen atoms surrounding the vacancies, forming a TCS complex (Fig. 3) [101,151,156,196,197]. EXAFS spectra fitting indicates that at low pH (pH ≈ 4.0), the Cu–Mn distance in the birnessite ranges from 3.39 Å to 3.43 Å, aligning with the Cu-TCS complex [63,156]. At high pH (pH ≈ 8.0), approximately 20 % of Cu^{2+} infiltrated the δ-MnO_2 layer (Cu INC) (Fig. 3), based on the peak near 2.9 Å in EXAFS spectral fitting and DFT calculation [63]. DFT studies conducted by Kwon et al. [150] explored the four-, five-, and six-fold Cu^{TCS} coordinations and suggested the existence of five or six O or OH in the first Cu shell.

With increasing Cu adsorption, more multinuclear Cu(II) clusters form at the periphery of manganite, particularly in the pH range of 3.3–5.3 [198]. Nevertheless, the stability of the twisted [CuO_6] octahedron is relatively low when subjected to proton attack under acidic conditions [198]. Similar to Ni and Pb, Cu binds to Mn octahedra at the birnessite's periphery through the edge or angular shared coordination [101,188]. EXAFS analysis by Peña et al. [196] showed that Cu predominantly attached to the periphery of birnessite in the configuration of dimers or polynuclear surface substances, with Cu favoring adsorption at particle edge more than Ni and Zn [196].

3.3.4. Cadmium

Surface complexation modeling indicates that the adsorption mechanism between Cd(II) and Mn oxide is mainly ion exchange at pH levels below 4.0 [199,200]. However, above pH 5.0, Cd^{2+} adsorbed onto birnessite shows similarities with Zn^{2+}, Cu^{2+}, and Ni^{2+}, with binding primarily occurring above and below octahedral vacancies [201], resulting in the formation of predominantly TCS inner-sphere complexes [62,186]. At pH 5.5, the addition of Mn(II) hinders the sorption of Cd(II) onto vacant sites, thereby forming DCS complexes at edge sites, suggesting that Cd(II) binds more strongly to vacant sites than edge sites [202].

3.3.5. Chromium

Cr(III) and Cr(VI) are the most commonly observed oxidation states of Cr. Under normal conditions, Cr(III) can only be oxidized by a limited number of natural oxidants, such as Mn oxides [203–206]. The adsorption capacity of Mn oxides for Cr is contingent upon their structure, composition, surface properties, and crystallinity [158,206]. Weaver and Hochella [175] quantitatively analyzed the oxidation kinetics of Cr across various Mn oxides, including hausmannite, manganite, romanechite, cryptomelane, lithiophorite, pyrolusite, and birnessite, finding birnessite most effective converting Cr(III) to Cr(VI). Further comparative studies on Cr(III) reactivity in various Mn oxides confirmed that the oxidation rate of birnessite was the most rapid [147]. The hydration tendency (pK_1) of the heavy metals, the surface variable charge of the Mn minerals, and pH significantly impact the adsorption [147].

Previous research outlines a three-step process for the oxidation of Cr(III) by birnessite. Initially, Cr(III) present in the solution enters the vacancies in the octahedral layers of MnO_6, then undergoes redox reactions with adjacent Mn(IV), releasing Cr(VI) into the solution [207]. Nevertheless, an alternative hypothesis suggests that Cr(III) does not penetrate a vacancy prior to oxidation but instead undergoes electron transfer with Mn oxide when forming the outer-sphere complex, thereby generating octahedral coordinated Cr(IV). This Cr(IV) either infiltrates vacancies, while the remaining fraction undergoes a configuration metamorphosis to generate tetrahedrally coordinated Cr(IV), which is expeditiously oxidized by Mn oxide to Cr(V) and Cr(VI) [175,208]. EXAFS analysis shows Cr(III) adsorption as a strong inner-sphere complex, while Cr(VI) adsorbs weakly onto Mn(IV)O_2 as an outer-sphere complex [209]. Recent studies indicate both Cr(III) and Cr(VI) can form inner-sphere complexes at birnessite's octahedral sites when the pH exceeds PZC [210].

3.3.6. Cobalt

The oxidation of Co(II) on the surface of hexagonal Mn oxides occurs via two potential mechanisms: (1) initially, the Mn(III) in the Mn oxide layers undergoes a disproportionation reaction, creating octahedral vacancies. Subsequently, Co(II) adsorbs above and below the octahedral vacancies and undergoes immediate oxidation to Co(III) by adjacent layer Mn(III), which then occupies the vacancies (Fig. 4). This reduces Mn(III) to Mn(II), which then either migrates to the interlayer or enters the solution, forming new octahedral vacancies. The total number of vacancies remains constant throughout this process [211–214]. (2) The second mechanism involves the initial oxidation of Co(II) in the solution to Co(III) by interlayer Mn(III) situated above and below the octahedral vacancy, followed by the reduction of interlayer Mn(III) to Mn(II) which subsequently enters the solution (Fig. 4). Here, Mn(III) acts as an electron acceptor with higher oxidizing potential than Mn(IV). Co(III) replaces Mn(III) at the octahedral vacancies, reducing the quantity of vacancies [59,215,216].

Previous research indicates Co(II) adsorption onto Mn oxides, including birnessite, cryptomelane, and pyrolusite, occurs in two phases: rapid adsorption and slow adsorption [218–220]. The former phase is governed by the mechanism (1), wherein Co(II) undergoes adsorption and oxidation at particle edges, forming Co^{2+}-DCS and Co^{3+}-DES complexes (Fig. 3) [100]. Edge Mn(III) acts as the most efficient oxidizing agent in this phase [100]. However, Manceau and Steinmann [217] posited that the oxidation of Co(II) does not occur at the edge of the MnO_2 layers but is adsorbed onto Mn(IV) vacancies on layers surfaces as TCS complex (Fig. 3). Subsequently, Co(II) enters the vacancies and undergoes oxidation to form Co(III) by the layer Mn(IV) cations [201]. The slow phase may follow mechanism (2), where interlayer Mn(III) slowly oxidizes Co(II) to Co(III). Due to the higher crystal field stabilization energy, Co(III) incorporates into the lattice through isomorphic substitution, releasing Mn(II) into the solution, illustrating the distinct behavior of Co(III) and Mn(III) in the system [212,218,221].

4. Factors affecting the sorption and oxidation of metals on Mn oxides

The adsorption of metal ions onto Mn oxides is significantly influenced by the intrinsic properties of the Mn oxides, including their oxidation state, surface charge, crystallinity, and surface area, as well as the physical and chemical characteristics of the metal elements. Moreover, a range of environmental factors, such as reactant concentration, temperature, reaction time, pH value, and coexisting ions, also influence the adsorption behavior and capacity of Mn oxides for metal ions [8,116,222].

4.1. Phase, size and morphology

The performance of Mn oxides is significantly influenced by their phase, size, and morphology [223]. Layered Mn oxides are categorized into triclinic and hexagonal structures based on structural symmetry [129,224], while common tunneled Mn oxides possess n × m structures [116–122]. Hexagonal birnessites, consist of curled layers of edge-sharing [Mn(IV)O_6] and [Mn(III)O_6] octahedra with varying amounts of octahedral vacancies, possessing superior oxidation capacity compared to the triclinic birnessites [225].

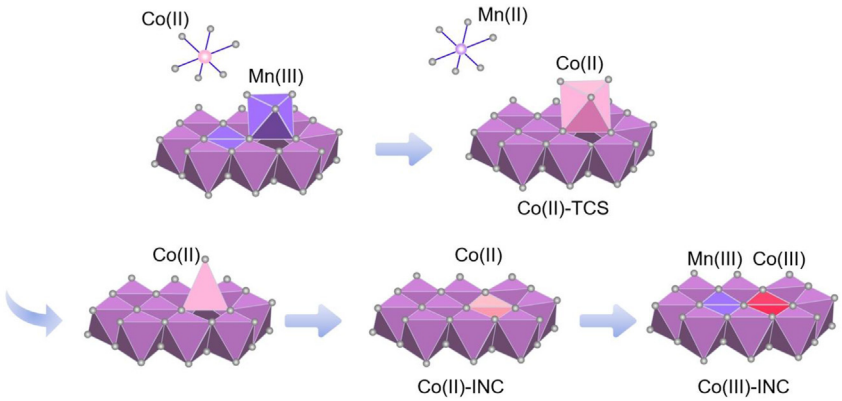

Fig. 4. Reaction mechanism of oxidative adsorption of cobalt on hexagonal birnessite. The transformation of the octahedral TCS complex into a smaller tetrahedral TCS complex facilitates the migration of Co(II) through the surface oxygen layer and its subsequent occupation of the vacant octahedral Mn(IV) site. Upon occupying the octahedral vacancy, Co(II) undergoes a transition from the high-spin to the low-spin state, accompanied by a significant distortion of the Co(II) octahedron due to the Jahn–Teller effect. Subsequently, an electron exchange reaction occurs between Mn(IV) and Co(II), leading to the formation of a regular low-spin Co(III) octahedron and a Jahn–Teller distorted high-spin Mn(III) octahedron. Adapted with permission from ref. [217]. Copyright 2022, American Chemical Society. TCS, triple-corner-sharing.

The Mn oxides possess distinct Mn–O coordination configuration numbers due to their varying phase structures. Metal substitution in the layer depends on the coordination radius (CR) with Mn(III)/Mn(IV) [201]. Surface energies of cryptomelane, Na-birnessite, K-birnessite, and Ca-birnessite are significantly lower than binary Mn oxides (Mn_3O_4, Mn_2O_3, and MnO_2), indicating enhanced stability of layered and tunneled structures at the nanoscale. Surface energies decrease with the average Mn oxidation state. Additionally, the transformation between Mn oxide phases with increasing surface area tends to favor compositions with lower surface energy [226].

Natural Mn oxides are commonly present in soil and water sediments as surface coatings or small particle aggregates, exhibiting a large specific surface area, especially for layered Mn oxides and Mn oxides with large tunnel sizes [1,20,227], which also have substantial inner surface, usually occupied by moisture and metal ions [38,40]. Mineral phases, such as δ-MnO_2, randomly stacked birnessite, and acidic birnessite, characterized by poor crystallinity and layered structure, exhibit strong metal adsorption and oxidation capabilities [228]. Birnessites with higher amorphousness, for example, possessed a remarkable adsorption capacity for Cr(III), surpassing that of pyrolusite, hausmannite, and manganite. Pyrolusite displayed a comparatively lower adsorption capacity, potentially attributable to its elevated crystallinity [148]. δ-MnO_2, with fewer layers and greater specific surface area than acidic birnessite, adsorbs a greater quantity of metal ions such as Tl(I) prior to the transition from a layered to tunneled structure [91].

The specific surface area of natural Mn oxides varies with crystal structure type, and differences even exist within the same structure type. Even Mn oxides synthesized through the identical methods can exhibit considerable variation in specific surface area. For instance, birnessites synthesized under alkaline conditions can have surface areas ranging from 120 to 315 m^2/g [93,159,229,230].

4.2. pH

pH significantly affects the hydrolysis of metal ions, ion exchange between metal and hydrogen ions, surface charge adsorption, and metal ion distribution in reaction system [14,147,231]. Mn oxides, categorized as hydrate oxide types [232], exhibit cation adsorption capacity determined by hydroxyl sites [233,234]. The surface of Mn oxides in suspension exhibits variable charges strongly influenced by the medium's pH value [147,148], with increasing pH leading to a more negative surface charge (Fig. 5). Hence, the zero point of charge (PZC) is crucial in assessing Mn oxides' adsorption capacity for metal cations, with PZC values varying across different structures [235,236]. In the soil Mn minerals, the PZC ranges from 1.5 in birnessite to 7 in Hausmannite [237,238], indicating the potential for a substantial negative surface charge in soil pH conditions [236].

When the pH value is below the pH_{PZC}, the hydroxyl group (≡MnOH) on the surface of Mn oxides tends to form positively charged $\equiv MnOH_2^+$ through protonation reactions, still enabling metal ion adsorption. Conversely, when the pH value exceeds the pH_{PZC}, the surface ≡Mn–OH reacts with OH^- to form negatively charged $\equiv MnO^-$ groups, with metal ions adsorption influenced by hydroxyl complexation and electrostatic attraction [113,239]. Aguilar-Carrillo et al. [113] discovered that the adsorption capacity of Tl^+ onto birnessite was greater at pH = 6 than pH = 2, attributed to birnessite's more negative charge near neutral pH, enhancing Tl affinity. Higher Cr(VI) production from Cr(III) oxidation by birnessite at pH 2.0 and 3.0 compared to pH 4.0 and 5.0 is due to surface charge alterations below PZC, birnessite dissolution at pH ≤ 3.5, and increased redox potential of birnessite at low pH [36,240].

Nevertheless, the pH-independent chemical adsorption and the high metal ion affinity to Mn oxides regardless of surface charge are observed. Metal ion adsorption order on Mn oxides is generally consistent with the hydroxylated cation stability, with Pb^{2+} exhibiting the highest affinity, followed by $Cu^{2+} > Co^{2+} > Ni^{2+} > Zn^{2+} > Mn^{2+} > Ca^{2+} > Mg^{2+} > Na^+$ [58,147,152,153]. The reduction in the average charge of metal cations resulting from hydrolysis leads to a significant decrease in their secondary hydration energy. This, in turn, lowers the energy barrier that hydroxylated cations must overcome during specific adsorption onto the oxide surface, thereby facilitating adsorption [147,175].

The pH level also plays a significant role in determining the configuration and structural transformation of Mn oxides [79,164,241,242]. For instance, δ-MnO_2 transforms to γ-MnO_2 at pH 2.4, α-MnO_2 at pH 4, α-MnOOH at pH 6, and γ-MnOOH at pH 8.0 [241,242]. Under conditions of pH 7.0–8.5 and high Mn(II)/MnO_2 ratios, birnessite transforms into feitknechtite (γ-MnOOH), manganite (γ-MnOOH), and hausmannite (Mn_3O_4) [44]. These transformations impact heavy metal immobilization or mobilization, consequently altering their environmental behaviors.

4.3. Valence states of Mn and octahedral vacancies

4.3.1. Valence states of Mn

The adsorption capacity for various metal ions, including Pb^{2+}, Cu^{2+}, Zn^{2+}, and Cd^{2+}, increases with the average oxidation state (AOS) of Mn, indicating stronger binding energy and affinity as higher AOS (Fig. 6) [62]. A highly significant linear positive correlation between the

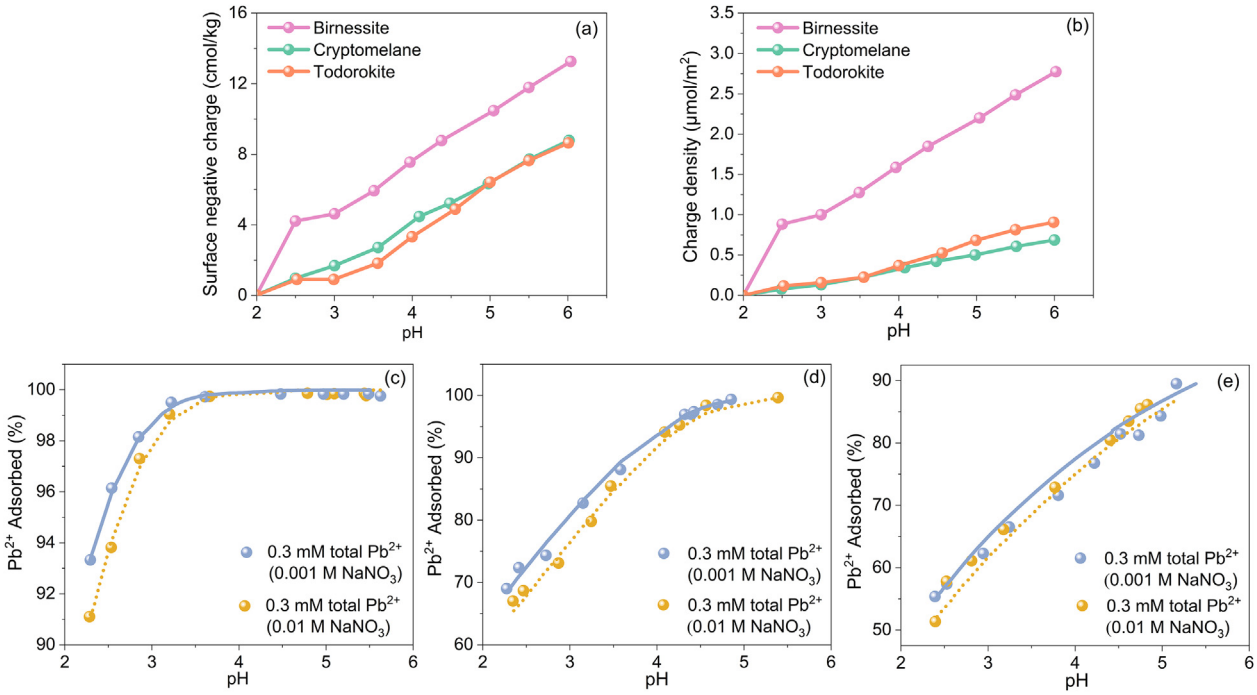

Fig. 5. Relationship between pH and surface charge, charge density, and adsorption amount of Pb^{2+} of different MnO_2. (**a**) Surface negative charge; (**b**) charge density; (**c**) birnessite sample (Mn_{AOS} = 3.92), (**d**) birnessite sample (Mn_{AOS} = 3.83); (**e**) birnessite sample (Mn_{AOS} = 3.67). AOS is the abbreviation for the average oxidation state of Mn. The dotted line and the solid line represent the Pb^{2+} adsorption amount calculated by the CD-MUSIC-EDL model at 0.001 mol/L and 0.01 mol/L ionic strength, respectively. Data used in (a) and (b) are from the study by Feng et al. [147], and data used in (c), (d), and (e) are from the study by Zhao et al. [177].

AOS and the maximum adsorption capacity of Pb^{2+} was observed (Fig. 6) [177].

Mn(IV) is the primary oxidant in Mn oxide systems [182,184]. Birnessites and todorokite, possessing the highest Mn(IV) content (showing high AOS), exhibit greater oxidation rates for metal ions of variable valence, whereas lithiophorite, characterized by a higher Mn(III) content (exhibiting relatively low AOS), displays the lowest oxidation rate [158,206]. The oxidation rate of Cr(III) increases with the AOS of birnessite [147,206]. This phenomenon can be attributed to the higher proportion of Mn(IV) in Mn oxide minerals (Fig. 6), which is advantageous for enhancing the oxidation of Cr(III) [147]. Zhang et al. [160] synthesized vernadite with varying AOS but identical particle sizes, finding that vernadite with lower AOS exhibited a reduced oxidation rate for As(III).

Contrarily, some studies highlight the significant oxidation capabilities of Mn(III) [59,180,206]. Mn(III) may enhance oxidative reactions through two mechanisms: first, the redox potential of Mn(III) → Mn(II) surpasses that of Mn(IV) → Mn(III), which greatly enhances electron transfer to Mn oxides in solid–liquid systems [211]; second, Mn(III) and the corresponding reduction products form inner-sphere complexes more quickly on the oxide surface compared to Mn(IV) [243]. Studies show that Mn(III) is crucial in Cr(III) oxidation in δ-MnO_2 [180], and the presence of Mn(II) and/or Mn(III) impurities within the Mn(IV)O_2 structure may augment the mineral's capacity to oxidize Cr(III) [177,228]. In natural environments, dissolved Mn(III) binds to various organic or inorganic ligands to form complexes with different stabilities. In forest top soils, reactive Mn(III) species dominate the oxidative activity [177].

Although Mn(IV) exhibits greater oxidation capability than Mn(III), their oxidation rate towards variable valence metals can differ. Therefore, further comprehensive investigation is required to elucidate the underlying mechanisms involved.

4.3.2. *Octahedral vacancies*

Octahedral vacancies predominantly occur within the layered Mn oxides, such as birnessite, resulting from the deficiency of center Mn in [MnO_6] octahedron in the layers. Many studies have indicated that the birnessite structural vacancies account for the negative layer charges [62,147,154,177]. Therefore, the quantity of octahedral vacancies significantly impacts the affinity and adsorption capacity of Mn oxides towards metals, as well as their oxidation potential for variable valence metals [85].

The correlation between the AOS of Mn in birnessites and the interplanar distance of the *d*110 crystal surface lattice reveals that an increase in AOS correlates with more octahedral vacancies [62,154,177]. The increase of vacancies in the Mn oxide layer leads to a corresponding increase in the quantity of hydroxyl groups bound to them, thereby facilitating the formation of surface complexes between metal ions and surface hydroxyl groups. The presence of additional octahedral vacancies in birnessite layers facilitates the selective adsorption of particular metal ions, especially those that form stable complexes with unsaturated O(H) groups in a tridentate coordination mode on the vacancies [48,129].

The existence of interlayer Mn(III)/Mn(II) also influences the adsorption capability of Mn oxides towards metals. Studies have demonstrated that Pb^{2+} substituted Mn^{3+} situated above/below the octahedral vacancies between layers during the adsorption process. Interlayer Mn^{3+} ions can undergo disproportionation reactions, leading to the incorporation of Mn^{4+} into the octahedral vacancies. This process resulted in a reduction in the number of octahedral vacancies and subsequently diminished the adsorption capacity of Pb^{2+} [244].

4.4. *The concentration of the initial reactants*

Variations in the initial concentrations of reactants can modify the coverage of the active sites on the surface of Mn oxides, impacting their adsorption/oxidation capacity for metals and potentially altering the overall reaction mechanism [48,147]. When the quantity of Mn oxide is fixed, the number of active sites typically remains constant. However, as the initial concentration of metal ions increases, the total amount of metal adsorption also rises [147]. Consequently, within a certain metal concentration range, the adsorbent can exhibit significant effectiveness. For example, increases in concentrations of Pb^{2+}, Cu^{2+}, Co^{2+}, Cd^{2+}, and Zn^{2+} lead to enhanced absorption on birnessite, todorokite,

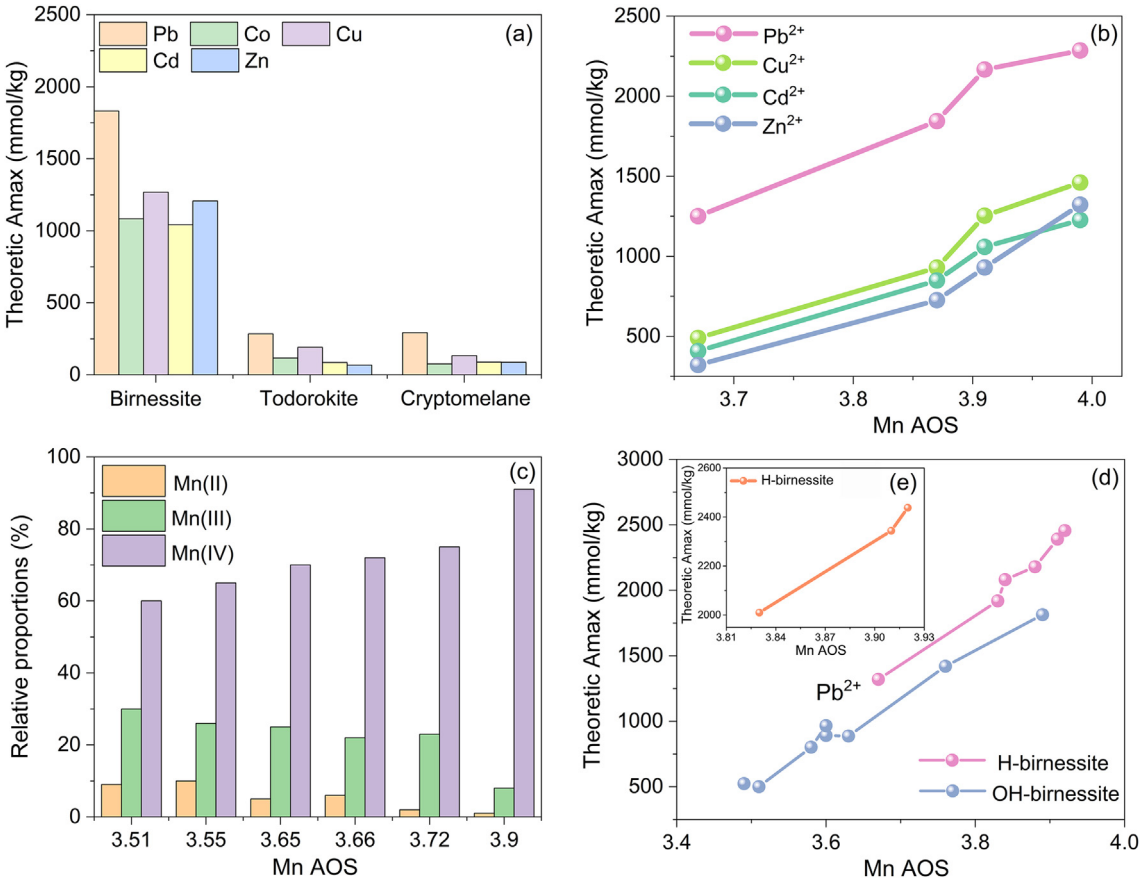

Fig. 6. The relationship between Mn AOS and adsorption capacity for metal ions. (**a**) Three different MnO_2; (**b**) birnessites with the same structure but different AOS; (**c**) relative proportions of Mn(II), Mn(III) and Mn(IV) in birnessite with different Mn AOS; (**d**) adsorption of lead ions by H-birnessite and OH-birnessite with different Mn AOS; (**e**) Adsorption of lead ions by H-birnessite with different Mn AOS. Data used in (a) are from the study by Feng et al. [147]; data used in (b) are from the study by Wang et al. [62]; data used in (c) are from Wu et al. [123]; data used in (d) are from Zhao et al. [155]; data used in (e) are from the study by Zhao et al. [154]. AOS, average oxidation state.

cryptomelane, and hausmannite, depending on the specific metal species and minerals [8].

With a higher concentration of Mn oxides, there is a corresponding increase in the total surface area, active adsorption sites, and the likelihood of contact between Mn oxides and metal ions, resulting in more rapid metal ion capture. Increasing the solid concentration of birnessite notably enhances the oxidation rate of As(III) and the adsorption capacity for As(V) [183,185]. However, at excessively high Mn oxide dosage, the crowding effect can hinder metal ions from reaching the adsorption sites, known as the solid concentration effect [245].

Extensive research has focused on the adsorption or redox effects of Mn oxides on common transition metals like Zn, Pb, Cu, Cr, and Co, among others. Yet, there is limited research on specific metals or metalloids, such as Sb and Tl, which are highly toxic biologically and can be indicators of paleoceanographic and paleoclimate [129,246,247]. Ruiz Garcia et al. [91] found that the addition of small quantities of Tl(I) to hexagonal birnessite in multiple instances differs significantly from a single addition of the same total amount. The former approach transformed birnessite into a tunnel-structured Mn oxide, whereas the latter did not change the structure. In the stepwise addition scenario, water might act as a reducing agent for Mn oxides [91]. However, the exact mechanism for the thalliomelane-like $[Tl^{+}(Mn_{7.5}^{4+}Cu_{0.5}^{2+})O_{16}]$ stepwise formation requires further investigation.

4.5. Doped and pre-adsorbed metal ions

Mn oxide minerals in natural environments are often rich in various metallic elements, including K, Ca, Zn, Co, Ni, and V [11,37,57,162]. The sequestration of these metals by Mn oxides can be classified into two situations: the incorporation of metal ions (substitution) during the genesis of Mn oxides, or the adsorption of metal ions onto the pre-existing Mn oxides [248]. Previous studies have shown that the metal ion inclusion in Mn oxides alters their microstructure, physicochemical properties, and reactivity. These alterations include alterations in crystal thickness along the *c** axis, coherent scattering domain size in the *a-b* plane, layer symmetry, particle size, specific surface area, Mn AOS, vacancy content, surface hydroxyl number, and even mineral structure transformation. Consequently, these modifications affect the adsorption and oxidation properties of the Mn oxides for metals [78,149,190,198,224,249,250].

The adsorption sites for metal ions post-doping depend on the dopant type. Most doped metal ions are adsorbed to vacancies and particle edge sites, with a minor integration into the octahedral layer [198]. The doped ions occupying the initial octahedral vacancies lead to a reduced number of available vacancies. Despite the increase in substrate surface and edge sites due to reduced thickness along the *c** axis, the augmented edge sites are inadequate to offset the occupied sites, reducing the metal adsorption capacity [59]. However, Co-doped birnessites exhibit enhanced Pb^{2+} removal compared to undoped versions [161], attributed to negative charge acquisition in the octahedral layer from Mn(IV) substitution with Co(III), and vacancy creation due to heterogeneity between Co(III) and Mn^{4+}/Mn^{3+} (Fig. 7a, c). Conversely, in Co pre-adsorbed birnessite, Co(III) incorporation and Mn^{3+}/Mn^{2+} adsorption on vacancies reduce the number of available vacancies and edge sites, decreasing metal adsorption capacity (Fig. 7b, d) [250]. In Ni-doped birnessite, significant Ni(II) occupation of vacancies and edge positions further reduces vacancy availability [162]. Nevertheless, specific metal ions can form

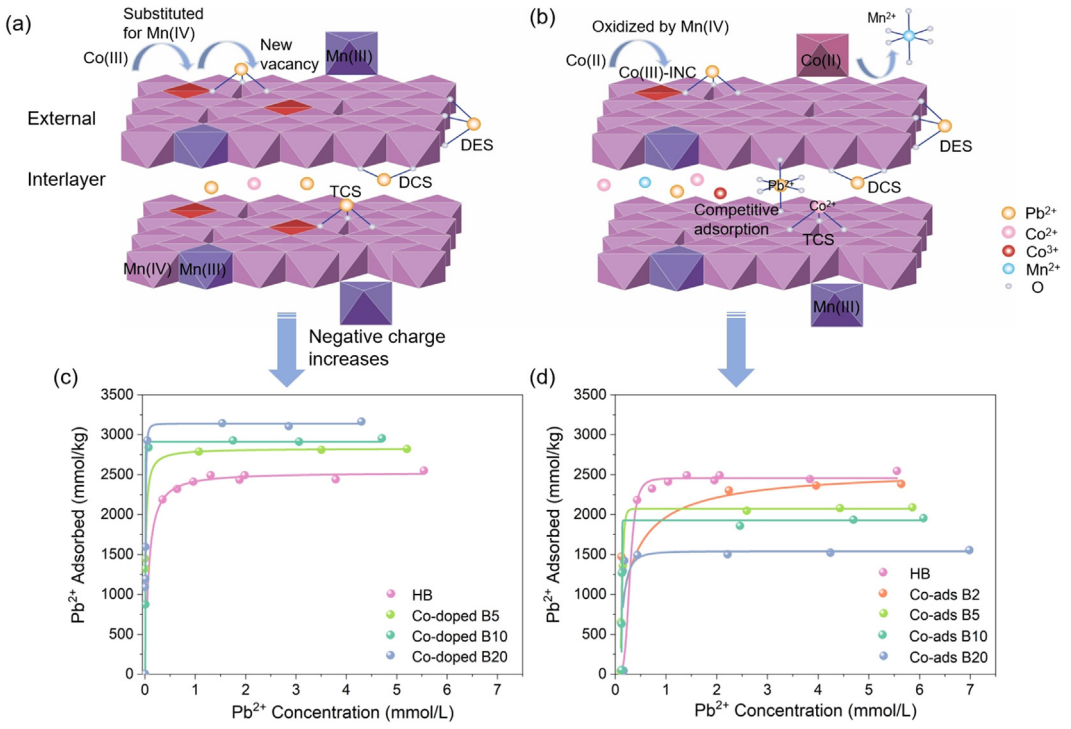

Fig. 7. The mechanisms and isothermal curves of Pb^{2+} uptake by Co-doped birnessites and Co pre-adsorbed birnessite. (**a**) Mechanism for Co-doped birnessites; (**b**) mechanism for Co pre-adsorbed birnessite; (**c**) isothermal curve for Co-doped birnessites; (**d**) isothermal curve for Co pre-adsorbed birnessite. In (c), based on the initial molar ratios of Co/Mn as 0, 0.05, 0.10, and 0.20, the products were named HB, Co-doped B5, Co-doped B10, and Co-doped B20. Accordingly, the products were named HB, Co-ads B2, Co-ads B5, Co-ads B10, and Co-ads B20 in (d), respectively. Data used in this figure are from the study by Yin et al. [161] and Yin et al. [250]. The X-ray absorption fine structure (XAFS) spectra of these birnessite samples were measured on the 1W1B beamline at the Beijing Synchrotron Radiation Facility.

complexes at the edge sites of birnessite, increasing adsorption capacity when doped with these ions. For example, V-doped birnessite shows increased vacancy content and decreased particle size with rising V content, imparting a large negative charge and enhancing the adsorption capacity [190].

The oxidation of variable valence metals by Mn oxides is impacted by the presence of doped metals, which can modify the structural composition and alter the oxidizing properties of Mn oxides. For example, when Na^{+} and Ca^{2+} are coprecipitated with Mn(II) in birnessite formation, the mineral's symmetry shifts from hexagonal to triclinic. This transformation influences the overall distribution of Mn ions and consequently reduces birnessite's oxidation capacity [214]. The introduction of V (VO_x^{n-}) into cryptomelane as a substitute for Mn(IV) gradually lowers the Mn AOS, reducing the mineral's oxidation resistance [57]. Similarly, adding Co to birnessite leads to isomorphic substitution of Mn(III) by Co(III), reducing the Jahn Teller distorted Mn(III) octahedron in the mineral and disrupting the transition from birnessite to todorokite, thus preventing oxidation capacity [34]. Doping birnessite with Pb(II) decreases the initial rate of As(III) oxidation due to the blockage of edge sites by Pb(II) [191]. The co-precipitation of Ni^{2+} and Mn^{2+} increases octahedral vacancies, facilitating the formation of hexagonal birnessite and enhancing its oxidation [214]. Zn^{2+} doping in birnessite's layers dynamically reduces Mn(III) in the layers, creating new vacancies, reducing particle size, and consequently enhancing adsorption and oxidation properties [192,251]. In experimental conditions, Ni^{2+}-doped birnessite showed superior oxidation ability compared to undoped birnessite, resulting in a rapid initial reaction rate that completes the oxidation of As(III) in solution [162].

4.6. Synergistic effects of multiple factors in real environments

Current research on Mn oxides' impact on metal adsorption and oxidation mechanisms mainly involves single-factor experiments, with a limited number of orthogonal experiments. In the natural environment, a variety of chemical, biological, and geological factors simultaneously influence the adsorption, oxidation, and immobilization of metal ions, often displaying synergistic or antagonistic effects. Additionally, microorganisms, like bacteria and fungi, can actively engage in the transformation of Mn oxides through their life processes and secretions [199, 252–254]. Moreover, owing to their pronounced reactivity and extensive widespread presence, Mn oxides often interact with multiple heavy metals such as lead, nickel, cadmium, zinc, and antimony, among others, within the natural environment [201].

Simulating natural conversion pathways in the laboratory remains challenging due to limited experimental data. For instance, reproducing todorokite under low temperatures and neutral environmental conditions in the lab is difficult. The current methods for synthesizing todorokite from layered Mn oxides typically require conditions that significantly differ from those in nature, such as elevated pH levels [18, 105,255,256]. The aforementioned observation outcome exhibits a notable disparity from the prevailing occurrence of todorokite in naturally occurring low-temperature settings [18]. Therefore, accurately replicating Mn oxides' adsorption and oxidation mechanisms on metals, along with their key influencing factors, is complicated in real-world scenarios.

5. Conclusions and prospects

Decades of research have led to a thorough understanding of the genesis, classifications, and structural characteristics of Mn oxides in nature, though comprehensive reviews on these subjects are limited. Islam et al. [8] focused predominantly on the synthesis and characterization of Mn oxides, placing specific emphasis on the kinetics, thermodynamics, and adsorption capacity of various metals. Shi et al. [79] reviewed the transformation pathways of birnessite and the mechanisms of heavy metal stabilization during this transformation process. Chen

et al. [201] categorized metal adsorption on Mn oxides into surface adsorption, lattice replacement, and formation of association minerals. Furthermore, they also discussed the synthesis of Mn composites based on synergy and water treatment applications.

Compared to the aforementioned review, our review delves deeper into the adsorption and redox reactions between Mn oxides and trace metals at a more microscopic level. This is achieved by incorporating insights from various analytical methods, including X-ray absorption fine structure spectroscopy (XAFS), X-ray photoelectron spectroscopy, XRD, nuclear magnetic resonance, infrared spectrometer (IR), DFT, and so on. Our main conclusions are outlined accordingly.

Birnessites, a type of layered Mn oxide, are characterized by low crystallinity, significant specific surface area, and low PZC, endowing them with numerous adsorption sites capable of adsorbing metal ions over a broad pH range. Hexagonal birnessites, in particular, demonstrate superior oxidation potential for metals with variable valence states due to their high AOS and abundant octahedral vacancies. In contrast, tunneled Mn oxides with relatively higher crystallinity and constrained by ion hydration radius and tunnel dimensions show reduced metal adsorption capacity and greater selectivity.

Through the utilization of advanced instrumental analysis techniques, researchers have acquired a certain comprehension of the binding modes between various metal ions and Mn oxides. For example, XAFS helps ascertain the metal ions' valence state and local coordination environments. The combination of extended EXAFS and DFT offers deeper insight into metal ion locations, such as whether they are adsorbed on octahedral vacancies in layered Mn oxides, inter-layered, or located in tunnels of tunneled Mn oxides, or adsorbed on the edge sites of mineral particles, including their coordination modes like TCS, DCS, DES, among others.

The adsorption/oxidation behavior and mechanisms of Mn oxides towards metals have been explored under various internal and external environmental conditions: (1) specifically, for layered Mn oxides, the number of octahedral vacancies and Mn(IV) ratio may influence adsorption capacity more than a large specific surface area; (2) the effect of pH on adsorption and oxidation capacities largely hinges on the PZC of Mn oxides; (3) reactant concentration significantly affects the adsorption/oxidation reaction, influencing the metal (Me)/Mn molar ratio post-adsorption, which can fundamentally alter the oxidative adsorption mechanism and potentially induce mineral transformation; (4) coprecipitated or pre-adsorbed metal ions during Mn oxide formation can impact Mn oxides' capacity to adsorb/oxidize other metal ions; (5) layered Mn oxides, with higher specific surface areas and Mn ion oxidation states, show greater adsorption and oxidation capacities than tunnel Mn oxides. However, tunnel structures offer more stability, making metal ions within less likely to be released.

Despite extensive research on Mn oxides' adsorption/oxidation mechanisms for metals, some aspects remain unclear. We have outlined several directions for future research to address these uncertainties.

(1) Research on Mn oxides' interactions with less abundant, toxic metals like thallium (Tl) [49,91,129,257] and antimony (Sb) [189,258–262] is limited and warrants further exploration.

(2) The role of photocatalysis on the redox activity of Mn oxides with metals, particularly in the presence of organic substances or other minerals, is not well understood and warrants further investigation.

(3) The precise adsorption mechanisms for variable valence metals on Mn oxides, particularly under varying Me/Mn loading ratios, need clarification. For instance, prior research has indicated that, under low Tl/Mn loading, the quantity of electrons transferred by Tl(I) does not correspond with the number of electrons received by Mn(IV). It is plausible that the oxidation of Tl(I) may instigate the reduction of Mn(IV) by H_2O [91], although this mechanism has yet to be fully understood.

(4) While the geometric coordination modes of metals on Mn oxides are known, precise characterization of these modes, particularly atomic distances in different structures are similar, remains challenging. For instance, DCS and DES complexes of Pb on hexagonal birnessite are difficult to distinguish from TCS complexes [162]. Accurate identifying of these coordination states is essential for understanding the environmental release and migration mechanisms of metals.

(5) The isotopic compositions of metals exhibit significant variability, rendering them useful as tracers for elucidating their origin, transfer, and biogeochemical cycling [263], as well as for investigating environmental and paleoceanographic phenomena [134,264,265]. In recent times, the advent of multi-collector inductively coupled plasma mass spectrometry has enabled precise determination of isotopic compositions for specific elements, and thereby enhances our comprehension of elemental geochemistry. Nevertheless, the impact of Mn oxide mineralogy on metal isotopic fractionation during adsorption is under-researched, necessitating further research.

(6) The structural transformation of natural Mn oxides, influenced by various chemical, biological, and geological factors, needs further exploration. For example, the dissolution and metal release under redox conditions, non-selective adsorption due to coexisting metals, and organic compound interactions with Mn oxides are areas needing more clarity. Quantifying the contributions of different pathways in complex scenarios remains a challenge.

(7) Comprehensive research on the coexistence of multiple heavy metals in complex systems is crucial. This includes understanding the adsorption priority based on metal toxicity, developing selective adsorption materials tailored to different metals, and exploiting synergistic relationships between metals for simultaneous adsorption, creating more effective remediation strategies.

Author contributions

F.L.: methodology, formal analysis, investigation, data curation, writing–original draft, writing–review & editing. H.Y.: conceptualization, methodology, investigation, data curation, project administration, writing–review & editing. T.Q.Z.: investigation, writing–review & editing. W.Z.: conceptualization, methodology, supervision, project administration, funding acquisition, formal analysis, investigation, data curation, writing–original draft, writing–review & editing.

Declaration of competing interests

The authors declare that they have no known competing financial interests or personal relationships that could have appeared to influence the work reported in this paper.

Acknowledgments

We owe great thanks to Dr. Lirong Zheng at Beamline 1W1B at Beijing Synchrotron Radiation Facility (BSRF) for the theoretical and technical support. W. Z greatly thanks the Laoshan Laboratory Science and Technology Innovation Project (No. LSKJ202205003) and the Natural Science Foundation of Shandong Province, China (No. ZR2020MD074). H. Y. greatly thanks the Natural Science Foundations of China (No. 42077015).

Appendix A. Supplementary data

Supplementary data to this article can be found online at https://doi.org/10.1016/j.eehl.2024.01.002.

References

[1] Y. Vodyanitskii, Mineralogy and geochemistry of manganese: a review of publications, Eurasian Soil Sci. 42 (2009) 1170–1178, https://doi.org/10.1134/S1064229309100123.
[2] J.E. Post, Manganese oxide minerals: crystal structures and economic and environmental significance, Proc. Natl. Acad. Sci. U. S. A. 96 (1999) 3447–3454, https://doi.org/10.1073/pnas.96.7.3447.
[3] G.J. Dick, B.G. Clement, S.M. Webb, F.J. Fodrie, J.R. Bargar, B.M. Tebo, Enzymatic microbial Mn(II) oxidation and Mn biooxide production in the Guaymas Basin

deep-sea hydrothermal plume, Geochim. Cosmochim. Acta 73 (2009) 6517–6530, https://doi.org/10.1016/j.gca.2009.07.039.
[4] A.A. Krylov, A. Hachikubo, H. Minami, T.V. Pogodaeva, T.I. Zemskaya, M.G. Krzhizhanovskaya, et al., Authigenic rhodochrosite from a gas hydrate-bearing structure in Lake Baikal, Int. J. Earth Sci. 107 (2018) 2011–2022, https://doi.org/10.1007/s00531-018-1584-z.
[5] M.J. Abernathy, M.V. Schaefer, C.J. Vessey, H. Liu, S.C. Ying, Oxidation of V(IV) by birnessite: kinetics and surface complexation, Environ. Sci. Technol. 55 (2021) 11703–11712, https://doi.org/10.1021/acs.est.1c02464.
[6] A. Manceau, M.A. Marcus, S. Grangeon, Determination of Mn valence states in mixed-valent manganates by XANES spectroscopy, Am. Mineral. 97 (2012) 816–827, https://doi.org/10.2138/am.2012.3903.
[7] V. Chakrapani, C. Wang, Q. Wang, N. Smieszek, Direct determination of Mn valence states in mixed-valent manganates by photoluminescence spectroscopy, Surf. Interface Anal. 54 (2022) 1192–1202, https://doi.org/10.1002/sia.7144.
[8] M.A. Islam, D.W. Morton, B.B. Johnson, B. Mainali, M.J. Angove, Manganese oxides and their application to metal ion and contaminant removal from wastewater, J. Water Process Eng. 26 (2018) 264–280, https://doi.org/10.1016/j.jwpe.2018.10.018.
[9] K. Wen, O.A. Chadwick, P.M. Vitousek, E.L. Paulus, G. Landrot, R. V Tappero, et al., Manganese oxidation states in volcanic soils across annual rainfall gradients, Environ. Sci. Technol. 57 (2023) 730–740, https://doi.org/10.1021/acs.est.2c02658.
[10] X. Wang, G.J. Xie, N. Tian, C.C. Dang, C. Cai, J. Ding, et al., Anaerobic microbial manganese oxidation and reduction: a critical review, Sci. Total Environ. 822 (2022) 153513, https://doi.org/10.1016/j.scitotenv.2022.153513.
[11] B.M. Tebo, J.R. Bargar, B.G. Clement, G.J. Dick, K.J. Murray, D. Parker, et al., Biogenic manganese oxides: properties and mechanisms of formation, Annu. Rev. Earth Planet. Sci. 32 (2004) 287–328, https://doi.org/10.1146/annurev.earth.32.101802.120213.
[12] J.J. Morgan, Kinetics of reaction between O_2 and Mn(II) species in aqueous solutions, Geochim. Cosmochim. Acta 69 (2005) 35–48, https://doi.org/10.1016/j.gca.2004.06.013.
[13] Y. Wu, B. Deng, H. Xu, H. Konishi, Chromium(III) oxidation coupled with microbially mediated Mn(II) oxidation, Geomicrobiol. J. 22 (2005) 161–170, https://doi.org/10.1080/01490450590945997.
[14] K. Tanaka, Q. Yu, K. Sasaki, T. Ohnuki, Cobalt(II) oxidation by biogenic Mn oxide produced by *Pseudomonas* sp. Strain NGY-1, Geomicrobiol. J. 30 (2013) 874–885, https://doi.org/10.1080/01490451.2013.791352.
[15] C.M. Hansel, C.A. Zeiner, C.M. Santelli, S.M. Webb, Mn(II) oxidation by an ascomycete fungus is linked to superoxide production during asexual reproduction, Proc. Natl. Acad. Sci. U. S. A. 109 (2012) 12621–12625, https://doi.org/10.1073/pnas.1203885109.
[16] M. Villalobos, B. Toner, J. Bargar, G. Sposito, Characterization of the manganese oxide produced by pseudomonas putida strain MnB1, Geochim. Cosmochim. Acta 67 (2003) 2649–2662, https://doi.org/10.1016/S0016-7037(03)00217-5.
[17] S. Namgung, C.M. Chon, G. Lee, Formation of diverse Mn oxides: a review of bio/geochemical processes of Mn oxidation, Geosci. J. 22 (2018) 373–381, https://doi.org/10.1007/s12303-018-0002-7.
[18] H. Jung, M. Taillefert, J. Sun, Q. Wang, O.J. Borkiewicz, P. Liu, et al., Redox cycling driven transformation of layered manganese oxides to tunnel structures, J. Am. Chem. Soc. 142 (2020) 2506–2513, https://doi.org/10.1021/jacs.9b12266.
[19] A.J. Frierdich, E.A. Hasenmueller, J.G. Catalano, Composition and structure of nanocrystalline Fe and Mn oxide cave deposits: implications for trace element mobility in karst systems, Chem. Geol. 284 (2011) 82–96, https://doi.org/10.1016/j.chemgeo.2011.02.009.
[20] J.E. Post, D.R. Veblen, Crystal structure determinations of synthetic sodium, magnesium, and potassium birnessite using TEM and the Rietveld method, Am. Mineral. 75 (1990) 477–489.
[21] R. Giovanoli, Vernadite is random-stacked birnessite, Miner. Depos. 15 (1980) 251–253, https://doi.org/10.1007/bf00206520.
[22] S. Lee, H. Xu, XRD and tem studies on nanophase manganese oxides in freshwater ferromanganese nodules from Green Bay, Lake Michigan, Clays Clay Miner. 64 (2016) 523–536, https://doi.org/10.1346/CCMN.2016.064032.
[23] C. Burlet, Y. Vanbrabant, Study of the spectro-chemical signatures of cobalt-manganese layered oxides (asbolane-lithiophorite and their intermediates) by Raman spectroscopy, J. Raman Spectrosc. 46 (2015) 941–952, https://doi.org/10.1002/jrs.4755.
[24] B. Zachau-Christiansen, K. West, T. Jacobsen, S. Skaarup, Insertion of lithium into the manganese dioxides: pyrolusite and ramsdellite, Solid State Ionics 70–71 (1994) 401–406, https://doi.org/10.1016/0167-2738(94)90344-1.
[25] I. Tsuyumoto, T. Moriguchi, Synthesis and lithium insertion properties of ramsdellite $LixTiO_2$ anode materials, Mater. Res. Bull. 70 (2015) 748–752, https://doi.org/10.1016/j.materresbull.2015.06.014.
[26] A.A. Ali, F.A. Al-Sagheer, M.I. Zaki, Surface texture of microcrystalline tunnel-structured manganese(IV) oxides: nitrogen sorptiometry and electron microscopy studies, Adsorp. Sci. Technol. 20 (2002) 619–632, https://doi.org/10.1260/026361702760504314.
[27] J.E. Post, R.B. Von Dreele, P.R. Buseck, Symmetry and cation displacements in hollandites: structure refinements of hollandite, cryptomelane and priderite, Acta Crystallogr. B38 (1982) 1056–1065, https://doi.org/10.1107/s0567740882004968.
[28] J. Ostwald, Mineralogy of the Groote Eylandt manganese oxides: a review, Ore Geol. Rev. 4 (1988) 3–45, https://doi.org/10.1016/0169-1368(88)90003-0.
[29] J.E. Post, D.L. Bish, Rietveld refinement of the todorokite structure, Am. Mineral. 73 (1988) 861–869.
[30] T. Kohler, T. Armbruster, E. Libowitzky, Hydrogen bonding and Jahn–Teller distortion in groutite, α-MnOOH, and Manganite, γ-MnOOH, and their relations to the manganese dioxides ramsdellite and pyrolusite, J. Solid State Chem. 133 (1997) 486–500, https://doi.org/10.1006/jssc.1997.7516.
[31] K. Satomi, Oxygen positional parameters of tetragonal Mn_3O_4, J. Phys. Soc. Japan 16 (1961) 258–266, https://doi.org/10.1143/JPSJ.16.258.
[32] R.A. Robie, B.S. Hemingway, Low-temperature molar heat capacities and entropies of MnO_2 (pyrolusite), Mn_3O_4 (hausmanite), and Mn_2O_3 (bixbyite), J. Chem. Thermodyn. 17 (1985) 165–181, https://doi.org/10.1016/0021-9614(85)90069-2.
[33] S.M. Webb, B.M. Tebo, J.R. Bargar, Structural characterization of biogenic Mn oxides produced in seawater by the marine bacillus sp. strain SG-1, Am. Mineral. 90 (2005) 1342–1357, https://doi.org/10.2138/am.2005.1669.
[34] Z. Wu, C.L. Peacock, B. Lanson, H. Yin, L. Zheng, Z. Chen, et al., Transformation of Co-containing birnessite to todorokite: effect of Co on the transformation and implications for Co mobility, Geochim. Cosmochim. Acta 246 (2019) 21–40, https://doi.org/10.1016/j.gca.2018.11.001.
[35] Z. Wu, B. Lanson, X. Feng, H. Yin, Z. Qin, X. Wang, et al., Transformation of Ni-containing birnessite to tectomanganate: influence and fate of weakly bound Ni(II) species, Geochim. Cosmochim. Acta 271 (2020) 96–115, https://doi.org/10.1016/j.gca.2019.12.023.
[36] T.E. Flores-Guia, L.F. Cano Salazar, A. Martínez-Luévanos, J.A. Claudio-Rizo, Manganese oxides: synthesis and application as adsorbents of heavy metal ions, Handb. Nanomater. Nanocomposites Energy Environ. Appl. (2021) 2409–2428, https://doi.org/10.1007/978-3-030-36268-3_153.
[37] S. Bodeï, A. Manceau, N. Geoffroy, A. Baronnet, M. Buatier, Formation of todorokite from vernadite in Ni-rich hemipelagic sediments, Geochim. Cosmochim. Acta 71 (2007) 5698–5716, https://doi.org/10.1016/j.gca.2007.07.020.
[38] A.G. Newton, K.D. Kwon, Molecular simulations of hydrated phyllomanganates, Geochim. Cosmochim. Acta 235 (2018) 208–223, https://doi.org/10.1016/j.gca.2018.05.021.
[39] H. Yin, B. Lanson, S. Zhang, L. Liu, C.L. Peacock, J.E. Post, et al., Effect and fate of Ni during aging and thermal-induced phyllomanganate-to-tectomanganate transformation, Geochim. Cosmochim. Acta 333 (2022) 200–215, https://doi.org/10.1016/j.gca.2022.07.014.
[40] A.G. Newton, K.D. Kwon, Classical mechanical simulations of layer- and tunnel-structured manganese oxide minerals, Geochim. Cosmochim. Acta 291 (2020) 92–109, https://doi.org/10.1016/j.gca.2020.04.034.
[41] X. Wang, Y. Yang, L. Tao, M. He, Antimonite oxidation and adsorption onto two tunnel-structured manganese oxides: implications for antimony mobility, Chem. Geol. 579 (2021) 120336, https://doi.org/10.1016/j.chemgeo.2021.120336.
[42] D. Hou, D. O'Connor, A.D. Igalavithana, D.S. Alessi, J. Luo, D.C.W. Tsang, et al., Metal contamination and bioremediation of agricultural soils for food safety and sustainability, Nat. Rev. Earth Environ. 1 (2020) 366–381, https://doi.org/10.1038/s43017-020-0061-y.
[43] D.A. Ahmed, D.F. Slima, Heavy metal accumulation by *Corchorus olitorius* L. irrigated with wastewater, Environ. Sci. Pollut. Res. 25 (2018) 14996–15005, https://doi.org/10.1007/s11356-018-1675-1.
[44] Y. Li, X. Zhao, J. Wu, X. Gu, Surface complexation modeling of divalent metal cation adsorption on birnessite, Chem. Geol. 551 (2020) 119774, https://doi.org/10.1016/j.chemgeo.2020.119774.
[45] P. Yang, J.E. Post, Q. Wang, W. Xu, R. Geiss, P.R. McCurdy, et al., Metal adsorption controls stability of layered manganese oxides, Environ. Sci. Technol. 53 (2019) 7453–7462, https://doi.org/10.1021/acs.est.9b01242.
[46] S.C. Ying, B.D. Kocar, S. Fendorf, Oxidation and competitive retention of arsenic between iron- and manganese oxides, Geochim. Cosmochim. Acta 96 (2012) 294–303, https://doi.org/10.1016/j.gca.2012.07.013.
[47] I. Szlamkowicz, J. Stanberry, K. Lugo, Z. Murphy, M. Ruiz Garcia, L. Hunley, et al., Role of manganese oxides in controlling subsurface metals and radionuclides mobility: a review, ACS Earth Space Chem. 7 (2023) 1–10, https://doi.org/10.1021/acsearthspacechem.2c00113.
[48] B. Wan, R. Huang, J.M. Diaz, Y. Tang, Manganese oxide catalyzed hydrolysis of polyphosphates, ACS Earth Space Chem. 3 (2019) 2623–2634, https://doi.org/10.1021/acsearthspacechem.9b00220.
[49] S. Wick, J. Peña, A. Voegelin, Thallium sorption onto manganese oxides, Environ. Sci. Technol. 53 (2019) 13168–13178, https://doi.org/10.1021/acs.est.9b04454.
[50] W. Zhuang, M. Liu, J. Song, S.C. Ying, Retention of thallium by natural minerals: a review, Sci. Total Environ. 777 (2021) 146074, https://doi.org/10.1016/j.scitotenv.2021.146074.
[51] K. Tiede, T. Neumann, D. Stueben, Suitability of Mn-oxyhydroxides from Karst caves as filter material for drinking water treatment in Gunung Sewu, Indonesia, J. Soils Sediments 7 (2007) 53–58, https://doi.org/10.1065/jss2006.11.195.
[52] N.B. Singh, G. Nagpal, S. Agrawal, Rachna, Water purification by using adsorbents: a review, Environ. Technol. Innov. 11 (2018) 187–240, https://doi.org/10.1016/j.eti.2018.05.006.
[53] G. Crini, E. Lichtfouse, L.D. Wilson, N. Morin-Crini, Conventional and non-conventional adsorbents for wastewater treatment, Environ. Chem. Lett. 17 (2019) 195–213, https://doi.org/10.1007/s10311-018-0786-8.
[54] H. Shan, H. Mo, Y. Liu, C. Zeng, S. Peng, H. Zhan, As(III) removal by a recyclable granular adsorbent through dopping Fe-Mn binary oxides into graphene oxide

chitosan, Int. J. Biol. Macromol. 237 (2023) 124184, https://doi.org/10.1016/j.ijbiomac.2023.124184.
[55] B. Liu, D. Wang, H. Li, Y. Xu, L. Zhang, As(III) removal from aqueous solution using α-Fe_2O_3 impregnated chitosan beads with As(III) as imprinted ions, Desalination 272 (2011) 286–292, https://doi.org/10.1016/j.desal.2011.01.034.
[56] B.O. Otunola, O.O. Ololade, A review on the application of clay minerals as heavy metal adsorbents for remediation purposes, Environ. Technol. Innov. 18 (2020) 100692, https://doi.org/10.1016/j.eti.2020.100692.
[57] S. Mayanna, C.L. Peacock, F. Schäffner, A. Grawunder, D. Merten, E. Kothe, et al., Biogenic precipitation of manganese oxides and enrichment of heavy metals at acidic soil pH, Chem. Geol. 402 (2015) 6–17, https://doi.org/10.1016/j.chemgeo.2015.02.029.
[58] R.M. McKenzie, The adsorption of lead and other heavy metals on oxides of manganese and iron, Aust. J. Soil Res. 18 (1980) 61–73, https://doi.org/10.1071/SR9800061.
[59] A. Manceau, V.A. Drits, E. Silvester, C. Bartoli, B. Lanson, Structural mechanism of Co^{2+} oxidation by the phyllomanganate buserite, Am. Mineral. 82 (1997) 1150–1175, https://doi.org/10.2138/am-1997-11-1213.
[60] Z. Zhao, Y. Xiong, X. Cheng, X. Hou, Y. Yang, Y. Tian, et al., Adsorptive removal of trace thallium(I) from wastewater: a review and new perspectives, J. Hazard. Mater. 393 (2020) 122378, https://doi.org/10.1016/j.jhazmat.2020.122378.
[61] P. Zhao, Z. Huang, Q. Ma, B. Zhang, P. Wang, Artificial humic acid synthesized from food wastes: an efficient and recyclable adsorbent of Pb (II) and Cd (II) from aqueous solution, Environ. Technol. Innov. 27 (2022) 102399, https://doi.org/10.1016/j.eti.2022.102399.
[62] Y. Wang, X. Feng, M. Villalobos, W. Tan, F. Liu, Sorption behavior of heavy metals on birnessite: relationship with its Mn average oxidation state and implications for types of sorption sites, Chem. Geol. 292–293 (2012) 25–34, https://doi.org/10.1016/j.chemgeo.2011.11.001.
[63] D.M. Sherman, C.L. Peacock, Surface complexation of Cu on birnessite (δ-MnO_2): controls on Cu in the deep ocean, Geochim. Cosmochim. Acta 74 (2010) 6721–6730, https://doi.org/10.1016/j.gca.2010.08.042.
[64] S. Wang, D. Ye, X. Liu, H. Wang, W. Ma, H. Liu, Mn-Cr mixed oxide adsorbents with high SO_2 resistance for elemental mercury removal from coal-fired flue gas, J. Ind. Eng. Chem. 123 (2023) 260–271, https://doi.org/10.1016/j.jiec.2023.03.041.
[65] W. Xu, J.-M. Zhu, T.M. Johnson, X. Wang, Z.-Q. Lin, D. Tan, et al., Selenium isotope fractionation during adsorption by Fe, Mn and Al oxides, Geochim. Cosmochim. Acta 272 (2020) 121–136, https://doi.org/10.1016/j.gca.2020.01.001.
[66] M. Miletto, X. Wang, N.J. Planavsky, G.W. Luther, T.W. Lyons, B.M. Tebo, Marine microbial Mn(II) oxidation mediates Cr(III) oxidation and isotope fractionation, Geochim. Cosmochim. Acta 297 (2021) 101–119, https://doi.org/10.1016/j.gca.2021.01.008.
[67] J. Liu, J. Cao, W. Yuan, Q. Zhong, X. Xiong, Q. Ouyang, et al., Thallium adsorption on three iron (hydr)oxides and Tl isotopic fractionation induced by adsorption on ferrihydrite, Sci. Total Environ. 871 (2023) 161863, https://doi.org/10.1016/j.scitotenv.2023.161863.
[68] X. Li, Y. Tang, C. Han, Z. Wei, H. Fan, H. Lv, et al., A static tin–manganese battery with 30000-cycle lifespan based on stabilized Mn^{3+}/Mn^{2+} redox chemistry, ACS Nano 17 (2023) 5083–5094, https://doi.org/10.1021/acsnano.3c00242.
[69] C. Liu, X. Wang, X. Li, W. Cao, J. Yang, Detoxification of arsenite through adsorption and oxidative transformation on pyrolusite adsorption, Clean - Soil Air Water 40 (2012) 1265–1272, https://doi.org/10.1002/clen.201200027.
[70] W. Zhuang, J. Song, Thallium in aquatic environments and the factors controlling Tl behavior, Environ. Sci. Pollut. Res. 28 (2021) 35472–35487, https://doi.org/10.1007/s11356-021-14388-2.
[71] Y. Wang, S. Lin, L. Liu, F. Wang, X. Yang, G. Qiu, High-efficiency electrochemical removal of Cd(II) from wastewater using birnessite-biochar composites: performance and mechanism, Environ. Monit. Assess. 195 (2023) 549, https://doi.org/10.1007/s10661-023-11169-x.
[72] S.W. Lin, X. Yang, L.H. Liu, A.Y. Li, G.H. Qiu, Electrosorption of cadmium and arsenic from wastewaters using nitrogen-doped biochar: mechanism and application, J. Environ. Manage. 301 (2022) 113921, https://doi.org/10.1016/j.jenvman.2021.113921.
[73] H. Yin, L. Liu, J. Ma, C. Zhang, G. Qiu, Efficient removal of As(III) from groundwaters through self-alkalization in an asymmetric flow-electrode electrochemical separation system, Water Res. 246 (2023) 120734, https://doi.org/10.1016/j.watres.2023.120734.
[74] A.Z. Miller, A. Dionísio, M.A. Sequeira Braga, M. Hernández-Mariné, M.J. Afonso, V.S.F. Muralha, et al., Biogenic Mn oxide minerals coating in a subsurface granite environment, Chem. Geol. 322–323 (2012) 181–191, https://doi.org/10.1016/j.chemgeo.2012.07.005.
[75] C.M. Santelli, S.M. Webb, A.C. Dohnalkova, C.M. Hansel, Diversity of Mn oxides produced by Mn(II)-oxidizing fungi, Geochim. Cosmochim. Acta 75 (2011) 2762–2776, https://doi.org/10.1016/j.gca.2011.02.022.
[76] E. Silvester, A. Manceau, V.A. Drits, Structure of synthetic monoclinic Na-rich birnessite and hexagonal birnessite; II, Results from chemical studies and EXAFS spectroscopy, Am. Mineral. 82 (1997) 962–978, https://doi.org/10.2138/am-1997-9-1013.
[77] V.A. Drits, E. Silvester, A.I. Gorshkov, A. Manceau, Structure of synthetic monoclinic Na-rich birnessite and hexagonal birnessite: I. Results from X-ray diffraction and selected-area electron diffraction, Am. Mineral. 82 (1997) 946–961, https://doi.org/10.2138/am-1997-9-1012.
[78] H. Yin, J. Sun, X. Yan, X. Yang, X. Feng, W. Tan, et al., Effects of Co(II) ion exchange, Ni(II)- and V(V)-doping on the transformation behaviors of Cr(III) on hexagonal turbostratic birnessite-water interfaces, Environ. Pollut. 256 (2020) 113462, https://doi.org/10.1016/j.envpol.2019.113462.
[79] M. Shi, Q. Li, Q. Wang, X. Yan, B. Li, L. Feng, et al., A review on the transformation of birnessite in the environment: implication for the stabilization of heavy metals, J. Environ. Sci. 139 (2024) 496–515, https://doi.org/10.1016/j.jes.2023.06.019.
[80] A.-C. Gaillot, D. Flot, V.A. Drits, A. Manceau, M. Burghammer, B. Lanson, Structure of synthetic K-rich birnessite obtained by high-temperature decomposition of $KMnO_4$. I. Two-layer polytype from 800 °C experiment, Chem. Mater. 15 (2003) 4666–4678, https://doi.org/10.1021/cm021733g.
[81] C.L. Lopano, P.J. Heaney, J.E. Post, J. Hanson, S. Komarneni, Time-resolved structural analysis of K- and Ba-exchange reactions with synthetic Na-birnessite using synchrotron X-ray diffraction, Am. Mineral. 92 (2007) 380–387, https://doi.org/10.2138/am.2007.2242.
[82] C.L. Lopano, P.J. Heaney, J.E. Post, Cs-exchange in birnessite: reaction mechanisms inferred from time-resolved X-ray diffraction and transmission electron microscopy, Am. Mineral. 94 (2009) 816–826, https://doi.org/10.2138/am.2009.3068.
[83] H. Boumaiza, A. Renard, M. Rakotomalala Robinson, G. Kervern, L. Vidal, C. Ruby, et al., A multi-technique approach for studying Na triclinic and hexagonal birnessites, J. Solid State Chem. 272 (2019) 234–243, https://doi.org/10.1016/j.jssc.2019.02.017.
[84] M. Villalobos, B. Lanson, A. Manceau, B. Toner, G. Sposito, Structural model for the biogenic Mn oxide produced by Pseudomonas putida, Am. Mineral. 91 (2006) 489–502, https://doi.org/10.2138/am.2006.1925.
[85] A.C. Gaillot, V.A. Drits, A. Manceau, B. Lanson, Structure of the synthetic K-rich phyllomanganate birnessite obtained by high-temperature decomposition of $KMnO_4$. Substructures of K-rich birnessite from 1000 °C experiment, Microporous Mesoporous Mater. 98 (2007) 267–282, https://doi.org/10.1016/j.micromeso.2006.09.010.
[86] J.E. Post, P.J. Heaney, J. Hanson, Rietveld refinement of a triclinic structure for synthetic Na-birnessite using synchrotron powder diffraction data, Powder Diffr. 17 (2002) 218–221, https://doi.org/10.1154/1.1498279.
[87] B. Lanson, V.A. Drits, Q. Feng, A. Manceau, Structure of synthetic Na-birnessite: evidence for a triclinic one-layer unit cell, Am. Mineral. 87 (2002) 1662–1671, https://doi.org/10.2138/am-2002-11-1215.
[88] J.P. Lefkowitz, E.J. Elzinga, Structural alteration of hexagonal birnessite by aqueous Mn(II): impacts on Ni(II) sorption, Chem. Geol. 466 (2017) 524–532, https://doi.org/10.1016/j.chemgeo.2017.07.002.
[89] S. Park, K.D. Kwon, Atomistic insights into the interlayer cation and water structures of Na-, K-, and Cs-birnessite, ACS Earth Space Chem. 5 (2021) 3159–3169, https://doi.org/10.1021/acsearthspacechem.1c00259.
[90] R.M. McKenzie, The synthesis of birnessite, cryptomelane, and some other oxides and hydroxides of manganese, Mineral. Mag. 38 (1971) 493–502, https://doi.org/10.1180/minmag.1971.038.296.12.
[91] M. Ruiz-Garcia, M. Villalobos, A. Voegelin, T. Pi-Puig, N. Martínez-Villegas, J. Göttlicher, Transformation of hexagonal birnessite upon reaction with thallium(I): effects of birnessite crystallinity, pH, and thallium concentration, Environ. Sci. Technol. 55 (2021) 4862–4870, https://doi.org/10.1021/acs.est.0c07886.
[92] L.S. Balistrieri, J.W. Murray, The surface chemistry of δ-MnO_2 in major ion sea water, Geochim. Cosmochim. Acta 46 (1982) 1041–1052, https://doi.org/10.1016/0016-7037(82)90057-6.
[93] J.W. Murray, The surface chemistry of hydrous manganese dioxide, J. Colloid Interface Sci. 46 (1974) 357–371, https://doi.org/10.1016/0021-9797(74)90045-9.
[94] L. Jiang, P. Wu, Y. Xu, Y. Li, M. Chen, Z. Ahmed, et al., Impacts of ammonium ion on triclinic birnessites towards the transformation of As(III), Environ. Pollut. 298 (2022) 118815, https://doi.org/10.1016/j.envpol.2022.118815.
[95] S. Grangeon, B. Lanson, M. Lanson, A. Manceau, Crystal structure of Ni-sorbed synthetic vernadite: a powder X-ray diffraction study, Mineral. Mag. 72 (2008) 1279–1291, https://doi.org/10.1180/minmag.2008.072.6.1279.
[96] S. Grangeon, F. Warmont, C. Tournassat, B. Lanson, M. Lanson, E. Elkaïm, et al., Nucleation and growth of feitknechtite from nanocrystalline vernadite precursor, Eur. J. Mineral 29 (2017) 767–776, https://doi.org/10.1127/ejm/2017/0029-2665.
[97] S. Lee, H. Xu, W. Xu, X. Sun, The structure and crystal chemistry of vernadite in ferromanganese crusts, Acta Crystallogr. Sect. B Struct. Sci. Cryst. Eng. Mater. 75 (2019) 591–598, https://doi.org/10.1107/S2052520619006528.
[98] S. Grangeon, A. Fernandez-Martinez, F. Warmont, A. Gloter, N. Marty, A. Poulain, et al., Cryptomelane formation from nanocrystalline vernadite precursor: a high energy X-ray scattering and transmission electron microscopy perspective on reaction mechanisms, Geochem. Trans. 16 (2015) 12, https://doi.org/10.1186/s12932-015-0028-y.
[99] S. Lee, H. Xu, Using complementary methods of synchrotron radiation powder diffraction and pair distribution function to refine crystal structures with high quality parameters — a review, Minerals 10 (2020) 124, https://doi.org/10.3390/min10020124.
[100] A.A. Simanova, K.D. Kwon, S.E. Bone, J.R. Bargar, K. Refson, G. Sposito, et al., Probing the sorption reactivity of the edge surfaces in birnessite nanoparticles using nickel(II), Geochim. Cosmochim. Acta 164 (2015) 191–204, https://doi.org/10.1016/j.gca.2015.04.050.
[101] A. Manceau, M. Lanson, N. Geoffroy, Natural speciation of Ni, Zn, Ba, and As in ferromanganese coatings on quartz using X-ray fluorescence, absorption, and diffraction, Geochim. Cosmochim. Acta 71 (2007) 95–128, https://doi.org/10.1016/j.gca.2006.08.036.

[102] A.L. Atkins, S. Shaw, C.L. Peacock, Nucleation and growth of todorokite from birnessite: implications for trace-metal cycling in marine sediments, Geochim. Cosmochim. Acta 144 (2014) 109–125, https://doi.org/10.1016/j.gca.2014.08.014.
[103] S. Ching, J.P. Franklin, C.M. Spencer, Cr-hollandite: breaking tradition with todorokite-type manganese oxides, Polyhedron 58 (2013) 53–59, https://doi.org/10.1016/j.poly.2012.07.099.
[104] S. Yun, H. Hwang, G. Hwang, Y. Kim, D. Blom, T. Vogt, et al., Super-hydration and reduction of manganese oxide minerals at shallow terrestrial depths, Nat. Commun. 13 (2022) 1–8, https://doi.org/10.1038/s41467-022-29328-y.
[105] H. Cui, F. Liu, X. Feng, W. Tan, M.K. Wang, Aging promotes todorokite formation from layered manganese oxide at near-surface conditions, J. Soils Sediments 10 (2010) 1540–1547, https://doi.org/10.1007/s11368-010-0261-z.
[106] F.A. Al-Sagheer, M.I. Zaki, Synthesis and surface characterization of todorokite-type microporous manganese oxides: implications for shape-selective oxidation catalysts, Microporous Mesoporous Mater. 67 (2004) 43–52, https://doi.org/10.1016/j.micromeso.2003.10.005.
[107] A. Manceau, S. Llorca, G. Calas, Crystal chemistry of cobalt and nickel in lithiophorite and asbolane from New Caledonia, Geochim. Cosmochim. Acta 51 (1987) 105–113, https://doi.org/10.1016/0016-7037(87)90011-1.
[108] F.V. Chukhrov, V.A. Drits, A.I. Gorshkov, Structural transformations of manganese oxides in oceanic nodules, Int. Geol. Rev. 29 (1987) 110–121, https://doi.org/10.1080/00206818709466128.
[109] M. Aoshima, Y. Tani, R. Fujita, K. Tanaka, N. Miyata, K. Umezawa, Simultaneous sequestration of Co^{2+} and Mn^{2+} by fungal manganese oxide through asbolane formation, Minerals 12 (2022) 358, https://doi.org/10.3390/min12030358.
[110] J. Sánchez-España, I. Yusta, Coprecipitation of Co^{2+}, Ni^{2+} and Zn^{2+} with Mn(III/IV) oxides formed in metal-rich mine waters, Minerals 9 (2019) 226, https://doi.org/10.3390/min9040226.
[111] Y.N. Vodyanitskii, A.A. Vasil'ev, S.N. Lesovaya, E.F. Sataev, A.V. Sivtsov, Formation of manganese oxides in soils, Eurasian Soil Sci. 37 (2004) 572–584.
[112] N. Demirkiran, Copper adsorption by natural manganese dioxide, Trans. Nonferrous Met. Soc. China 25 (2015) 647–653, https://doi.org/10.1016/S1003-6326(15)63648-2.
[113] A. Sönmezay, M.S. Öncel, N. Bektaş, Adsorption of lead and cadmium ions from aqueous solutions using manganoxide minerals, Trans. Nonferrous Met. Soc. China 22 (2012) 3131–3139, https://doi.org/10.1016/S1003-6326(12)61765-8.
[114] Y. Fransiscus, C.V. Effendy, H.S. Wijaya, Effect of manganese coating on the sorption performance of pyrolusite for lead in aqueous conditions, IOP Conf. Ser. Mater. Sci. Eng. 742 (2020) 012005, https://doi.org/10.1088/1757-899X/742/1/012005.
[115] M. Pasero, A short outline of the tunnel oxides, Micro- Mesoporous Miner. Phases 57 (2018) 291–305, https://doi.org/10.2138/rmg.2005.57.9.
[116] P. Yadav, A. Bhaduri, A. Thakur, Manganese oxide nanoparticles: an insight into structure, synthesis and applications, ChemBioEng Rev. 10 (2023) 510–528, https://doi.org/10.1002/cben.202200056.
[117] S. Ching, K.S. Krukowska, S.L. Suib, A new synthetic route to todorokite-type manganese oxides, Inorg. Chim. Acta 294 (1999) 123–132, https://doi.org/10.1016/S0020-1693(99)00208-X.
[118] J. Gutzmer, N.J. Beukes, Mineralogy and mineral chemistry of oxide-facies manganese ores of the Postmasburg manganese field, South Africa, Mineral. Mag. 61 (1997) 213–231, https://doi.org/10.1180/minmag.1997.061.405.05.
[119] D.T.Q.J. Vicat, E. Fanchon, P. Strobel, The structure of $K_{1.33}Mn_8O_{16}$ and cation ordering in hollandite-type structures, Acta Cryst. 42 (1986) 162–167, https://doi.org/10.1107/s0108768186098415.
[120] M. Zhu, C.L. Farrow, J.E. Post, K.J.T. Livi, S.J.L. Billinge, M. Ginder-Vogel, et al., Structural study of biotic and abiotic poorly-crystalline manganese oxides using atomic pair distribution function analysis, Geochim. Cosmochim. Acta 81 (2012) 39–55, https://doi.org/10.1016/j.gca.2011.12.006.
[121] P. Yang, S. Lee, J.E. Post, H. Xu, Q. Wang, W. Xu, et al., Trivalent manganese on vacancies triggers rapid transformation of layered to tunneled manganese oxides (TMOs): implications for occurrence of TMOs in low-temperature environment, Geochim. Cosmochim. Acta 240 (2018) 173–190, https://doi.org/10.1016/j.gca.2018.08.014.
[122] D. Ma, J. Wu, P. Yang, M. Zhu, Coupled manganese redox cycling and organic carbon degradation on mineral surfaces, Environ. Sci. Technol. 54 (2020) 8801–8810, https://doi.org/10.1021/acs.est.0c02065.
[123] Z. Wu, B. Lanson, X. Feng, H. Yin, W. Tan, F. He, et al., Transformation of the phyllomanganate vernadite to tectomanganates with small tunnel sizes: favorable geochemical conditions and fate of associated Co, Geochim. Cosmochim. Acta 295 (2021) 224–236, https://doi.org/10.1016/j.gca.2020.12.021.
[124] J.E. Post, P.J. Heaney, J. Hanson, Synchrotron X-ray diffraction study of the structure and dehydration behavior of todorokite, Am. Mineral. 88 (2003) 142–150, https://doi.org/10.2138/am-2003-0117.
[125] D.A. McKeown, J.E. Post, Characterization of manganese oxide mineralogy in rock varnish and dendrites using X-ray absorption spectroscopy, Am. Mineral. 86 (2001) 701–713, https://doi.org/10.2138/am-2001-5-611.
[126] H.I. Kim, H.G. Cho, S. Lee, H.J. Koo, J.K. Hong, Y.K. Jin, Spatial distribution of manganese oxide minerals in the natural ferromanganese nodule of the Arctic Sea: a view from Raman spectroscopy, Chem. Geol. 623 (2023) 121398, https://doi.org/10.1016/j.chemgeo.2023.121398.
[127] J. Kim, K.D. Kwon, Tunnel cation and water structures of todorokite: insights into metal partitioning and isotopic fractionation, Geochim. Cosmochim. Acta 333 (2022) 153–165, https://doi.org/10.1016/j.gca.2022.07.008.
[128] H. Jung, C. Snyder, W. Xu, K. Wen, M. Zhu, Y. Li, et al., Photocatalytic oxidation of dissolved Mn^{2+} by TiO^2 and the formation of tunnel structured manganese oxides, ACS Earth Space Chem. 5 (2021) 2105–2114, https://doi.org/10.1021/acsearthspacechem.1c00154.
[129] C.L. Peacock, E.M. Moon, Oxidative scavenging of thallium by birnessite: explanation for thallium enrichment and stable isotope fractionation in marine ferromanganese precipitates, Geochim. Cosmochim. Acta 84 (2012) 297–313, https://doi.org/10.1016/j.gca.2012.01.036.
[130] A.L. Atkins, S. Shaw, C.L. Peacock, Release of Ni from birnessite during transformation of birnessite to todorokite: implications for Ni cycling in marine sediments, Geochim. Cosmochim. Acta 189 (2016) 158–183, https://doi.org/10.1016/j.gca.2016.06.007.
[131] X.H. Feng, M. Zhu, M. Ginder-Vogel, C. Ni, S.J. Parikh, D.L. Sparks, Formation of nano-crystalline todorokite from biogenic Mn oxides, Geochim. Cosmochim. Acta 74 (2010) 3232–3245, https://doi.org/10.1016/j.gca.2010.03.005.
[132] A. V Wegorzewski, S. Grangeon, S.M. Webb, C. Heller, T. Kuhn, Mineralogical transformations in polymetallic nodules and the change of Ni, Cu and Co crystal-chemistry upon burial in sediments, Geochim. Cosmochim. Acta 282 (2020) 19–37, https://doi.org/10.1016/j.gca.2020.04.012.
[133] Q. Yu, T. Ohnuki, N. Kozai, F. Sakamoto, K. Tanaka, K. Sasaki, Quantitative analysis of radiocesium retention onto birnessite and todorokite, Chem. Geol. 470 (2017) 141–151, https://doi.org/10.1016/j.chemgeo.2017.09.008.
[134] R.F. Phillips, Y. Wang, F. Klein, G. Farfan, C.M. Ostrander, H. Gadol, et al., The role of manganese oxide mineralogy in thallium isotopic fractionation upon sorption, Geochim. Cosmochim. Acta 356 (2023) 83–92, https://doi.org/10.1016/j.gca.2023.07.011.
[135] H. Kim, J. Kim, S.P. Hyun, K.D. Kwon, Toward a mechanistic understanding of cesium adsorption to todorokite: a molecular dynamics simulation study, J. Hazard. Mater. 436 (2022) 129250, https://doi.org/10.1016/j.jhazmat.2022.129250.
[136] D.Y. Chung, P.J. Heaney, J.E. Post, J.E. Stubbs, P.J. Eng, Synchrotron X-ray diffraction of pyrolusite (MnO_2) and rutile (TiO_2) during heating to ~1000 °C, J. Phys. Chem. Solids 177 (2023) 111284, https://doi.org/10.1016/j.jpcs.2023.111284.
[137] A.A. Bolzan, C. Fong, B.J. Kennedy, C.J. Howard, Powder neutron diffraction study of pyrolusite, β-MnO_2, Aust. J. Chem. 46 (1993) 939–944, https://doi.org/10.1071/CH9930939.
[138] P.E. Champness, The transformation manganite → pyrolusite, Mineral. Mag. 38 (1971) 245–248, https://doi.org/10.1180/minmag.1971.038.294.14.
[139] J.E. Post, P.J. Heaney, Neutron and synchrotron X-ray diffraction study of the structures and dehydration behaviors of ramsdellite and "groutellite", Am. Mineral. 89 (2004) 969–975, https://doi.org/10.2138/am-2004-0706.
[140] N.V. Chukanov, D.A. Varlamov, I.V. Pekov, N.V. Zubkova, A.V. Kasatkin, S.N. Britvin, Coupled substitutions in natural MnO(OH) polymorphs: Infrared spectroscopic investigation, Minerals 11 (2021) 1–13, https://doi.org/10.3390/min11090969.
[141] R.F. Korotkov, A.E. Baranchikov, O.V. Boytsova, A.E. Goldt, S.A. Kurzeev, V.K. Ivanov, Selective hydrothermal microwave synthesis of various manganese dioxide polymorphs, Russ. J. Inorg. Chem. 61 (2016) 129–134, https://doi.org/10.1134/S0036023616020091.
[142] O.S. Pokrovsky, J. Viers, R. Freydier, Zinc stable isotope fractionation during its adsorption on oxides and hydroxides, J. Colloid Interface Sci. 291 (2005) 192–200, https://doi.org/10.1016/j.jcis.2005.04.079.
[143] J.E. Post, D.L. Bish, Rietveld refinement of the coronadite structure, Am. Mineral. 74 (1989) 913–917.
[144] A. Byström, A.M. Byström, The crystal structure of hollandite, the related manganese oxide minerals, and α-MnO_2, Acta Crystallogr. 3 (1950) 146–154, https://doi.org/10.1107/s0365110x5000032x.
[145] J.E. Post, C.W. Burnham, Modeling tunnel-cation displacements in Hollandites using structure-energy calculations, Am. Mineral. 71 (1986) 1178–1185. Doi: 0003-004X/86/0910-117$02.00.
[146] R. Chitrakar, Y. Makita, A. Sonoda, Cesium adsorption by synthetic todorokite-type manganese oxides, Bull. Chem. Soc. Jpn. 87 (2014) 733–739, https://doi.org/10.1246/bcsj.20140017.
[147] X.H. Feng, L.M. Zhai, W.F. Tan, F. Liu, J.Z. He, Adsorption and redox reactions of heavy metals on synthesized Mn oxide minerals, Environ. Pollut. 147 (2007) 366–373, https://doi.org/10.1016/j.envpol.2006.05.028.
[148] M.A. Islam, M.J. Angove, D.W. Morton, B.K. Pramanik, M.R. Awual, A mechanistic approach of chromium (VI) adsorption onto manganese oxides and boehmite, J. Environ. Chem. Eng. 8 (2020) 103515, https://doi.org/10.1016/j.jece.2019.103515.
[149] H. Yin, F. Liu, X. Feng, T. Hu, L. Zheng, G. Qiu, et al., Effects of Fe doping on the structures and properties of hexagonal birnessites - comparison with Co and Ni doping, Geochim. Cosmochim. Acta 117 (2013) 1–15, https://doi.org/10.1016/j.gca.2013.04.020.
[150] K.D. Kwon, K. Refson, G. Sposito, Understanding the trends in transition metal sorption by vacancy sites in birnessite, Geochim. Cosmochim. Acta 101 (2013) 222–232, https://doi.org/10.1016/j.gca.2012.08.038.
[151] M. Villalobos, J. Bargar, G. Sposito, Mechanisms of Pb(II) sorption on a biogenic manganese oxide, Environ. Sci. Technol. 39 (2005) 569–576, https://doi.org/10.1021/es049434a.
[152] G. Fu, H.E. Allen, C.E. Cowan, Adsorption of cadmium and copper by manganese oxide, Soil Sci. 152 (1991) 72–81, https://doi.org/10.1097/00010694-19910800000002.
[153] C.J. Matocha, E.J. Elzinga, D.L. Sparks, Reactivity of Pb(II) at the Mn(III,IV) (oxyhydr)oxide−water interface, Environ. Sci. Technol. 35 (2001) 2967–2972, https://doi.org/10.1021/es0012164.
[154] W. Zhao, W. Tan, X. Feng, F. Liu, Y. Xie, Z. Xie, XAFS studies on surface coordination of Pb^{2+} on birnessites with different average oxidation states,

Colloids Surf. A Physicochem. Eng. Asp. 379 (2011) 86–92, https://doi.org/10.1016/j.colsurfa.2010.11.040.
[155] W. Zhao, X. Feng, W. Tan, F. Liu, S. Ding, Relation of lead adsorption on birnessites with different average oxidation states of manganese and release of $Mn^{2+}/H^{+}/K^{+}$, J. Environ. Sci. 21 (2009) 520–526, https://doi.org/10.1016/S1001-0742(08)62302-5.
[156] A. Manceau, B. Lanson, V.A. Drits, Structure of heavy metal sorbed birnessite. Part III: Results from powder and polarized extended X-ray absorption fine structure spectroscopy, Geochim. Cosmochim. Acta 66 (2002) 2639–2663, https://doi.org/10.1016/S0016-7037(02)00869-4.
[157] B. Lanson, V.A. Drits, A.-C. Gaillot, E. Silvester, A. Plançon, A. Manceau, Structure of heavy-metal sorbed birnessite: Part 1. Results from X-ray diffraction, Am. Mineral. 87 (2002) 1631–1645, https://doi.org/10.2138/am-2002-11-1213.
[158] J.G. Kim, J.B. Dixon, C.C. Chusuei, Y. Deng, Oxidation of chromium(III) to (VI) by manganese oxides, Soil Sci. Soc. Am. J. 66 (2002) 306–315, https://doi.org/10.2136/sssaj2002.3060.
[159] B.J. Lafferty, M. Ginder-Vogel, D.L. Sparks, Arsenite oxidation by a poorly crystalline manganese-oxide 1. stirred-flow experiments, Environ. Sci. Technol. 44 (2010) 8460–8466, https://doi.org/10.1021/es102013p.
[160] S. Zhang, S. Chen, F. Liu, J. Li, X. Liang, S. Chu, et al., Effects of Mn average oxidation state on the oxidation behaviors of As(III) and Cr(III) by vernadite, Appl. Geochem. 94 (2018) 35–45, https://doi.org/10.1016/j.apgeochem.2018.05.002.
[161] H. Yin, X. Feng, G. Qiu, W. Tan, F. Liu, Characterization of Co-doped birnessites and application for removal of lead and arsenite, J. Hazard. Mater. 188 (2011) 341–349, https://doi.org/10.1016/j.jhazmat.2011.01.129.
[162] H. Yin, W. Tan, L. Zheng, H. Cui, G. Qiu, F. Liu, et al., Characterization of Ni-rich hexagonal birnessite and its geochemical effects on aqueous Pb^{2+}/Zn^{2+} and As(III), Geochim. Cosmochim. Acta 93 (2012) 47–62, https://doi.org/10.1016/j.gca.2012.05.039.
[163] E.A. Johnson, J.E. Post, Water in the interlayer region of birnessite: importance in cation exchange and structural stability, Am. Mineral. 91 (2006) 609–618, https://doi.org/10.2138/am.2006.2090.
[164] C. Elmi, J.E. Post, P.J. Heaney, E.S. Ilton, Effects of pH and Ca exchange on the structure and redox state of synthetic Na-birnessite, Am. Mineral. 106 (2021) 15–27, https://doi.org/10.2138/am-2020-7112.
[165] H.Y. Zhao, X.R. Liang, H. Yin, F. Liu, W.F. Tan, G.H. Qiu, et al., Formation of todorokite from "c-disordered" H-birnessites: the roles of average manganese oxidation state and interlayer cations, Geochem. Trans. 16 (2015) 8, https://doi.org/10.1186/s12932-015-0023-3.
[166] L. Liu, Y. Luo, W. Tan, F. Liu, S.L. Suib, Y. Zhang, et al., Zinc removal from aqueous solution using a deionization pseudocapacitor with a high-performance nanostructured birnessite electrode, Environ. Sci. 4 (2017) 811–823, https://doi.org/10.1039/c6en00671j.
[167] X. Yang, L. Liu, W. Tan, G. Qiu, F. Liu, High-performance Cu^{2+} adsorption of birnessite using electrochemically controlled redox reactions, J. Hazard. Mater. 354 (2018) 107–115, https://doi.org/10.1016/j.jhazmat.2018.04.069.
[168] Q. Peng, L. Liu, Y. Luo, Y. Zhang, W. Tan, F. Liu, et al., Cadmium removal from aqueous solution by a deionization supercapacitor with a birnessite electrode, ACS Appl. Mater. Interfaces 8 (2016) 34405–34413, https://doi.org/10.1021/acsami.6b12224.
[169] J. Hai, L. Liu, W. Tan, R. Hao, G. Qiu, Catalytic oxidation and adsorption of Cr(III) on iron-manganese nodules under oxic conditions, J. Hazard. Mater. 390 (2020) 122166, https://doi.org/10.1016/j.jhazmat.2020.122166.
[170] L. Liu, Q. Qiao, W. Tan, X. Sun, C. Liu, Z. Dang, et al., Arsenic detoxification by iron-manganese nodules under electrochemically controlled redox: mechanism and application, J. Hazard. Mater. 403 (2021) 123912, https://doi.org/10.1016/j.jhazmat.2020.123912.
[171] T. Borch, R. Kretzschmar, A. Skappler, P. Van Cappellen, M. Ginder-Vogel, A. Voegelin, et al., Biogeochemical redox processes and their impact on contaminant dynamics, Environ. Sci. Technol. 44 (2010) 15–23, https://doi.org/10.1021/es9026248.
[172] A. Manceau, M.A. Marcus, N. Tamura, Quantitative speciation of heavy metals in soils and sediments by synchrotron X-ray techniques, Rev. Mineral. Geochem. 49 (2002), https://doi.org/10.2138/gsrmg.49.1.341.
[173] Z. Wang, D.E. Giammar, Metal contaminant oxidation mediated by manganese redox cycling in subsurface environment, ACS Symp. Ser. 1197 (2015) 29–50, https://doi.org/10.1021/bk-2015-1197.ch002.
[174] B.J. Lafferty, M. Ginder-Vogel, M. Zhu, K.J.T. Livi, D.L. Sparks, Arsenite oxidation by a poorly crystalline manganese-oxide. 2. results from X-ray absorption spectroscopy and X-ray diffraction, Environ. Sci. Technol. 44 (2010) 8467–8472, https://doi.org/10.1021/es102016c.
[175] R.M. Weaver, M.F. Hochella, The reactivity of seven Mn-oxides with Cr^{3+}aq: a comparative analysis of a complex, environmentally important redox reaction, Am. Mineral. 88 (2003) 2016–2027, https://doi.org/10.2138/am-2003-11-1246.
[176] M. Villalobos, The role of surface edge sites in metal(loid) sorption to poorly-crystalline birnessites, in: Advances in the Environmental Biogeochemistry of Manganese Oxides, American Chemical Society, 2015, pp. 4–65, https://doi.org/10.1021/bk-2015-1197.ch004 (Chapter 4).
[177] W. Zhao, W. Tan, M. Wang, J. Xiong, F. Liu, L. Weng, et al., CD-MUSIC-EDL modeling of Pb^{2+} adsorption on birnessites: role of Vacant and edge sites, Environ. Sci. Technol. 52 (2018) 10522–10531, https://doi.org/10.1021/acs.est.8b02644.
[178] F.F. Marafatto, B. Lanson, J. Peña, Crystal growth and aggregation in suspensions of δ-MnO_2 nanoparticles: implications for surface reactivity, Environ. Sci. Nano 5 (2017) 497–508, https://doi.org/10.1039/C7EN00817A.
[179] Z. Stepniewska, K. Bucior, R.P. Bennicelli, The effects of MnO_2 on sorption and oxidation of Cr(III) by soils, Geoderma 122 (2004) 291–296, https://doi.org/10.1016/j.geoderma.2004.01.015.
[180] P.S. Nico, R.J. Zasoski, Importance of Mn(III) availability on the rate of Cr(III) oxidation on δ-MnO_2, Environ. Sci. Technol. 34 (2000) 3363–3367, https://doi.org/10.1021/es991462j.
[181] M. Zhu, K.W. Paul, J.D. Kubicki, D.L. Sparks, Quantum chemical study of arsenic (III, V) adsorption on Mn-oxides: implications for arsenic(III) oxidation, Environ. Sci. Technol. 43 (2009) 6655–6661, https://doi.org/10.1021/es900537e.
[182] D. Banerjee, H.W. Nesbitt, Oxidation of aqueous Cr(III) at birnessite surfaces: constraints on reaction mechanism, Geochim. Cosmochim. Acta 63 (1999) 1671–1687, https://doi.org/10.1016/S0016-7037(99)00003-4.
[183] B.A. Manning, S.E. Fendorf, B. Bostick, D.L. Suarez, Arsenic(III) oxidation and Arsenic(V) adsorption reactions on synthetic birnessite, Environ. Sci. Technol. 36 (2002) 976–981, https://doi.org/10.1021/es0110170.
[184] H. Guha, J.E. Saiers, S. Brooks, P. Jardine, K. Jayachandran, Chromium transport, oxidation, and adsorption in manganese-coated sand, J. Contam. Hydrol. 49 (2001) 311–334, https://doi.org/10.1016/S0169-7722(00)00199-6.
[185] S.J. Parikh, B.J. Lafferty, T.G. Meade, D.L. Sparks, Evaluating environmental influences on As(III) oxidation kinetics by a poorly crystalline Mn-oxide, Environ. Sci. Technol. 44 (2010) 3772–3778, https://doi.org/10.1021/es903408g.
[186] C.M. Van Genuchten, J. Peña, Sorption selectivity of birnessite particle edges: a d-PDF analysis of Cd(II) and Pb(II) sorption by δ-MnO_2 and ferrihydrite, Environ. Sci. Process. Impacts 18 (2016) 1030–1041, https://doi.org/10.1039/c6em00136j.
[187] K.D. Kwon, K. Refson, G. Sposito, Surface complexation of Pb(II) by hexagonal birnessite nanoparticles, Geochim. Cosmochim. Acta 74 (2010) 6731–6740, https://doi.org/10.1016/j.gca.2010.09.002.
[188] Y. Takahashi, A. Manceau, N. Geoffroy, M.A. Marcus, A. Usui, Chemical and structural control of the partitioning of Co, Ce, and Pb in marine ferromanganese oxides, Geochim. Cosmochim. Acta 71 (2007) 984–1008, https://doi.org/10.1016/j.gca.2006.11.016.
[189] Q. Sun, P.X. Cui, C. Liu, S.M. Peng, M.E. Alves, D.M. Zhou, et al., Antimony oxidation and sorption behavior on birnessites with different properties (δ-MnO_2 and triclinic birnessite), Environ. Pollut. 246 (2019) 990–998, https://doi.org/10.1016/j.envpol.2018.12.027.
[190] H. Yin, X. Feng, W. Tan, L.K. Koopal, T. Hu, M. Zhu, et al., Structure and properties of vanadium(V)-doped hexagonal turbostratic birnessite and its enhanced scavenging of Pb^{2+} from solutions, J. Hazard. Mater. 288 (2015) 80–88, https://doi.org/10.1016/j.jhazmat.2015.01.068.
[191] M. Villalobos, I.N. Escobar-Quiroz, C. Salazar-Camacho, The influence of particle size and structure on the sorption and oxidation behavior of birnessite: I. Adsorption of As(V) and oxidation of As(III), Geochim. Cosmochim. Acta 125 (2014) 564–581, https://doi.org/10.1016/j.gca.2013.10.029.
[192] S. Grangeon, A. Manceau, J. Guilhermet, A.-C. Gaillot, M. Lanson, B. Lanson, Zn sorption modifies dynamically the layer and interlayer structure of vernadite, Geochim. Cosmochim. Acta 85 (2012) 302–313, https://doi.org/10.1016/j.gca.2012.02.019.
[193] Z. Wang, C. Peacock, K.D. Kwon, X. Gu, X. Feng, W. Li, Site-specific isotope fractionation during Zn adsorption onto birnessite: insights from X-ray absorption spectroscopy, density functional theory and surface complexation modeling, Geochim. Cosmochim. Acta 348 (2023) 68–84, https://doi.org/10.1016/j.gca.2023.03.006.
[194] K.D. Kwon, K. Refson, G. Sposito, Zinc surface complexes on birnessite: a density functional theory study, Geochim. Cosmochim. Acta 73 (2009) 1273–1284, https://doi.org/10.1016/j.gca.2008.11.033.
[195] M.-P. Isaure, A. Manceau, N. Geoffroy, A. Laboudigue, N. Tamura, M.A. Marcus, Zinc mobility and speciation in soil covered by contaminated dredged sediment using micrometer-scale and bulk-averaging X-ray fluorescence, absorption and diffraction techniques, Geochim. Cosmochim. Acta 69 (2005) 1173–1198, https://doi.org/10.1016/j.gca.2004.08.024.
[196] J. Peña, J.R. Bargar, G. Sposito, Copper sorption by the edge surfaces of synthetic birnessite nanoparticles, Chem. Geol. 396 (2015) 196–207, https://doi.org/10.1016/j.chemgeo.2014.12.021.
[197] Y. Li, F. Liu, X. Xu, Y. Liu, Y. Li, H. Ding, et al., Influence of heavy metal sorption pathway on the structure of biogenic birnessite: insight from the band structure and photostability, Geochim. Cosmochim. Acta 256 (2019) 116–134, https://doi.org/10.1016/j.gca.2018.12.008.
[198] Z. Qin, Q. Xiang, F. Liu, J. Xiong, L.K. Koopal, L. Zheng, et al., Local structure of Cu^{2+} in Cu-doped hexagonal turbostratic birnessite and Cu^{2+} stability under acid treatment, Chem. Geol. 466 (2017) 512–523, https://doi.org/10.1016/j.chemgeo.2017.06.040.
[199] X. Huang, T. Chen, X. Zou, M. Zhu, D. Chen, M. Pan, The adsorption of Cd(II) on manganese oxide investigated by batch and modeling techniques, Int. J. Environ. Res. Public Health 14 (2017) 1145, https://doi.org/10.3390/ijerph14101145.
[200] K. Suzuki, T. Kato, S. Fuchida, C. Tokoro, Removal mechanisms of cadmium by δ-MnO_2 in adsorption and coprecipitation processes at pH 6, Chem. Geol. 550 (2020) 119744, https://doi.org/10.1016/j.chemgeo.2020.119744.
[201] M. Chen, J. Wu, X. Qiu, L. Jiang, P. Wu, The important role of the interaction between manganese minerals and metals in environmental remediation: a review, Environ. Sci. Pollut. Res. 30 (2023) 39319–39337, https://doi.org/10.1007/s11356-023-25575-8.
[202] Q. Sun, P.X. Cui, M. Zhu, T.T. Fan, S.T. Ata-Ul-Karim, J.H. Gu, et al., Cd(II) retention and remobilization on δ-MnO_2 and Mn(III)-rich δ-MnO2 affected by Mn(II), Environ. Int. 130 (2019) 104932, https://doi.org/10.1016/j.envint.2019.104932.

[203] M. Chrysochoou, E. Theologou, N. Bompoti, D. Dermatas, I. Panagiotakis, Occurrence, origin and transformation processes of geogenic chromium in soils and sediments, Curr. Pollut. Rep. 2 (2016) 224–235, https://doi.org/10.1007/s40726-016-0044-2.

[204] D. Fandeur, F. Juillot, G. Morin, L. Olivi, A. Cognigni, S.M. Webb, et al., XANES evidence for oxidation of Cr(III) to Cr(VI) by Mn-oxides in a lateritic regolith developed on serpentinized ultramafic rocks of New Caledonia, Environ. Sci. Technol. 43 (2009) 7384–7390, https://doi.org/10.1021/es900498r.

[205] I. Reijonen, H. Hartikainen, Oxidation mechanisms and chemical bioavailability of chromium in agricultural soil–pH as the master variable, Appl. Geochem. 74 (2016) 84–93, https://doi.org/10.1016/j.apgeochem.2016.08.017.

[206] C. Negra, D.S. Ross, A. Lanzirotti, Oxidizing behavior of soil manganese, Soil Sci. Soc. Am. J. 69 (2005) 87–95, https://doi.org/10.2136/sssaj2005.0087a.

[207] A. Manceau, L. Charlet, X-ray absorption spectroscopic study of the sorption of Cr(III) at the oxide-water interface. I. Molecular mechanism of Cr(III) oxidation on Mn oxides, J. Colloid Interface Sci. 148 (1992) 425–442, https://doi.org/10.1016/0021-9797(92)90181-K.

[208] E. Silvester, L. Charlet, A. Manceau, Mechanism of chromium(III) oxidation by Na-buserite, J. Phys. Chem. 99 (1995) 16662–16669, https://doi.org/10.1021/j100045a028.

[209] G. Landrot, M. Ginder-Vogel, K. Livi, J.P. Fitts, D.L. Sparks, Chromium(III) oxidation by three poorly crystalline manganese(IV) oxides. 2. Solid phase analyses, Environ. Sci. Technol. 46 (2012) 11601–11609, https://doi.org/10.1021/es302384q.

[210] K.P. Kong, T.B. Fischer, P.J. Heaney, J.E. Post, J.E. Stubbs, P.J. Eng, Mineralogical and geochemical constraints on chromium oxidation induced by birnessite, Appl. Geochem. 108 (2019) 104365, https://doi.org/10.1016/j.apgeochem.2019.104365.

[211] E.J. Elzinga, A.B. Kustka, A Mn-54 radiotracer study of Mn isotope solid–liquid exchange during reductive transformation of vernadite (δ-MnO_2) by aqueous Mn(II), Environ. Sci. Technol. 49 (2015) 4310–4316, https://doi.org/10.1021/acs.est.5b00022.

[212] H. Zhao, X. Feng, S. Lee, B. Reinhart, E.J. Elzinga, Sorption and oxidation of Co(II) at the surface of birnessite: impacts of aqueous Mn(II), Chem. Geol. 618 (2023) 121281, https://doi.org/10.1016/j.chemgeo.2022.121281.

[213] J.R. Bargar, B.M. Tebo, U. Bergmann, S.M. Webb, P. Glatzel, V.Q. Chiu, et al., Biotic and abiotic products of Mn(II) oxidation by spores of the marine Bacillus sp. strain SG-1, Am. Mineral. 90 (2005) 143–154, https://doi.org/10.2138/am.2005.1557.

[214] M. Zhu, M. Ginder-Vogel, S.J. Parikh, X.-H. Feng, D.L. Sparks, Cation effects on the layer structure of biogenic Mn-oxides, Environ. Sci. Technol. 44 (2010) 4465–4471, https://doi.org/10.1021/es1009955.

[215] E. Hu, Y. Zhang, S. Wu, J. Wu, L. Liang, F. He, Role of dissolved Mn(III) in transformation of organic contaminants: non-oxidative versus oxidative mechanisms, Water Res. 111 (2017) 234–243, https://doi.org/10.1016/j.watres.2017.01.013.

[216] Y. Sun, J. Im, N. Shobnam, S.K. Fanourakis, L. He, L.M. Anovitz, et al., Degradation of adsorbed bisphenol A by soluble Mn(III), Environ. Sci. Technol. 55 (2021) 13014–13023, https://doi.org/10.1021/acs.est.1c03862.

[217] A. Manceau, S.N. Steinmann, Density functional theory modeling of the oxidation mechanism of Co(II) by birnessite, ACS Earth Space Chem. 6 (2022) 2063–2075, https://doi.org/10.1021/acsearthspacechem.2c00122.

[218] Y. Wang, S. Benkaddour, F.F. Marafatto, J. Pena, Diffusion- and pH-dependent reactivity of layer-type MnO2: reactions at particle edges versus vacancy sites, Environ. Sci. Technol. 52 (2018) 3476–3485, https://doi.org/10.1021/acs.est.7b05820.

[219] A.A. Simanova, J. Pena, Time-resolved investigation of cobalt oxidation by Mn(III)-rich δ-MnO_2 using quick X-ray absorption spectroscopy, Environ. Sci. Technol. 49 (2015) 10867–10876, https://doi.org/10.1021/acs.est.5b01088.

[220] C.C. Fuller, J.W. Harvey, Reactive uptake of trace metals in the hyporheic zone of a mining-contaminated stream, Pinal Creek, Arizona, Environ. Sci. Technol. 34 (2000) 1150–1155, https://doi.org/10.1021/es990714d.

[221] Q. Yu, K. Sasaki, K. Tanaka, T. Ohnuki, T. Hirajima, Structural factors of biogenic birnessite produced by fungus *Paraconiothyrium* sp. WL-2 strain affecting sorption of Co^{2+}, Chem. Geol. 310–311 (2012) 106–113, https://doi.org/10.1016/j.chemgeo.2012.03.029.

[222] M. Li, S. Kuang, Y. Kang, H. Ma, J. Dong, Z. Guo, Recent advances in application of iron-manganese oxide nanomaterials for removal of heavy metals in the aquatic environment, Sci. Total Environ. 819 (2022) 153157, https://doi.org/10.1016/j.scitotenv.2022.153157.

[223] H. Yan, D.H. Pi, S.Y. Jiang, J.W. Mao, L.G. Xu, X.Q. Yang, et al., Mineral paragenesis in Paleozoic manganese ore deposits: depositional versus post-depositional formation processes, Geochim. Cosmochim. Acta 325 (2022) 65–86, https://doi.org/10.1016/j.gca.2022.03.030.

[224] H. Yin, K.D. Kwon, J.Y. Lee, Y. Shen, H. Zhao, X. Wang, et al., Distinct effects of Al^{3+} doping on the structure and properties of hexagonal turbostratic birnessite: a comparison with Fe^{3+} doping, Geochim. Cosmochim. Acta 208 (2017) 268–284, https://doi.org/10.1016/j.gca.2017.03.040.

[225] Q. Wang, Z. Han, H. Liu, T. Chen, X. Zou, Z. Chu, et al., The pH-sensitive transformation of birnessite and its effect on the fate of norfloxacin, Chemosphere 341 (2023) 139932, https://doi.org/10.1016/j.chemosphere.2023.139932.

[226] N. Birkner, A. Navrotsky, Thermodynamics of manganese oxides: sodium, potassium, and calcium birnessite and cryptomelane, Abstr. Pap. Am. Chem. Soc. 114 (2017) E1046–E1053, https://doi.org/10.1073/pnas.1620427114.

[227] V.M. Burns, R.G. Burns, Post-depositional metal enrichment processes inside manganese nodules from the north equatorial Pacific, Earth Planet. Sci. Lett. 39 (1978) 341–348, https://doi.org/10.1016/0012-821X(78)90020-1.

[228] G. Landrot, M. Ginder-Vogel, K. Livi, J.P. Fitts, D.L. Sparks, Chromium(III) oxidation by three poorly-crystalline manganese(IV) oxides. 1. Chromium(III)-oxidizing capacity, Environ. Sci. Technol. 46 (2012) 11594–11600, https://doi.org/10.1021/es302383y.

[229] K.L. Godtfredsen, A.T. Stone, Solubilization of manganese dioxide-bound copper by naturally occurring organic compounds, Environ. Sci. Technol. 28 (1994) 1450–1458, https://doi.org/10.1021/es00057a012.

[230] W. Buser, P. Graf, Differenzierung von Mangan(II)-manganit und δ-MnO_2 durch Oberflächenmessung nach Brunauer-Emmet-Teller, Helv. Chim. Acta 38 (1955) 830–834, https://doi.org/10.1002/hlca.19550380327.

[231] Y. Xiong, X. Liu, H. Xiong, Aggregation modeling of the influence of pH on the aggregation of variably charged nanoparticles, Sci. Rep. 11 (2021) 1–10, https://doi.org/10.1038/s41598-021-96798-3.

[232] R.O. James, T.W. Healy, Adsorption of hydrolyzable metal ions at the oxide—water interface. III. A thermodynamic model of adsorption, J. Colloid Interface Sci. 40 (1972) 65–81, https://doi.org/10.1016/0021-9797(72)90174-9.

[233] K.P. Wang, Q. Liu, Adsorption of phosphorylated chitosan on mineral surfaces, Colloids Surf. A Physicochem. Eng. Asp. 436 (2013) 656–663, https://doi.org/10.1016/j.colsurfa.2013.07.030.

[234] K. Wu, T. Liu, C. Ma, B. Chang, R. Chen, X.C. Wang, The role of Mn oxide doping in phosphate removal by Al-based bimetal oxides: adsorption behaviors and mechanisms, Environ. Sci. Pollut. Res. 21 (2014) 620–630, https://doi.org/10.1007/s11356-013-1937-x.

[235] W.F. Tan, S.J. Lu, F. Liu, X.H. Feng, J.Z. He, L.K. Koopal, Determination of the point-of-zero charge of manganese oxides with different methods including an improved salt titration method, Soil Sci. 173 (2008) 277–286, https://doi.org/10.1097/SS.0b013e31816d1f12.

[236] R.M. McKenzie, The surface charge on manganese dioxides, Aust. J. Soil Res. 19 (1981) 41–50, https://doi.org/10.1071/SR9810041.

[237] M. Kosmulski, The pH-dependent surface charging and the points of zero charge, J. Colloid Interface Sci. 253 (2002) 77–87, https://doi.org/10.1006/jcis.2002.8490.

[238] S. Zhang, H. Li, Z. Wu, J.E. Post, B. Lanson, Y. Liu, et al., Effects of cobalt doping on the reactivity of hausmannite for As(III) oxidation and As(V) adsorption, J. Environ. Sci. 122 (2022) 217–226, https://doi.org/10.1016/j.jes.2022.02.004.

[239] L. Pietrelli, N.M. Ippolito, S. Ferro, V.G. Dovì, M. Vocciante, Removal of Mn and As from drinking water by red mud and pyrolusite, J. Environ. Manage. 237 (2019) 526–533, https://doi.org/10.1016/j.jenvman.2019.02.093.

[240] J. Aguilar-Carrillo, L. Herrera-García, I.A. Reyes-Domínguez, E.J. Gutiérrez, Thallium(I) sequestration by jarosite and birnessite: structural incorporation vs surface adsorption, Environ. Pollut. 257 (2020) 113492, https://doi.org/10.1016/j.envpol.2019.113492.

[241] M. Ao, S. Sun, T. Deng, F. Zhang, T. Liu, Y. Tang, Natural source of Cr (VI) in soil: the anoxic oxidation of Cr (III) by Mn oxides, J. Hazard. Mater. 433 (2022) 128805, https://doi.org/10.1016/j.jhazmat.2022.128805.

[242] Q. Zhang, Z. Xiao, X. Feng, W. Tan, G. Qiu, F. Liu, α-MnO_2 nanowires transformed from precursor δ-MnO_2 by refluxing under ambient pressure: the key role of pH and growth mechanism, Mater. Chem. Phys. 125 (2011) 678–685, https://doi.org/10.1016/j.matchemphys.2010.09.073.

[243] J.P. Lefkowitz, A.A. Rouff, E.J. Elzinga, Influence of pH on the reductive transformation of birnessite by aqueous Mn(II), Environ. Sci. Technol. 47 (2013) 10364–10371, https://doi.org/10.1021/es402108d.

[244] P.S. Nico, R.J. Zasoski, Mn(III) center availability as a rate controlling factor in the oxidation of phenol and sulfide on δ-MnO_2, Environ. Sci. Technol. 35 (2001) 3338–3343, https://doi.org/10.1021/es001848q.

[245] S. Zhang, B. Li, Y. Chen, M. Zhu, J.A. Pedersen, B. Gu, et al., Methylmercury degradation by trivalent manganese, Environ. Sci. Technol. 57 (2023) 5988–5998, https://doi.org/10.1021/acs.est.3c00532.

[246] W. Zhao, H. Cui, F. Liu, W. Tan, X. Feng, Relationship between Pb^{2+} adsorption and average Mn oxidation state in synthetic birnessites, Clays Clay Miner. 57 (2009) 513–520, https://doi.org/10.1346/CCMN.2009.0570501.

[247] W. Zhao, Q.Q. Wang, F. Liu, G.H. Qiu, W.F. Tan, X.H. Feng, Pb^{2+} adsorption on birnessite affected by Zn^{2+} and Mn^{2+} pretreatments, J. Soils Sediments 10 (2010) 870–878, https://doi.org/10.1007/s11368-010-0219-1.

[248] K.G. Bhattacharyya, S. Sen Gupta, Kaolinite and montmorillonite as adsorbents for Fe(III), Co(II) and Ni(II) in aqueous medium, Appl. Clay Sci. 41 (2008) 1–9, https://doi.org/10.1016/j.clay.2007.09.005.

[249] L. Ye, X. Meng, C. Jing, Influence of sulfur on the mobility of arsenic and antimony during oxic-anoxic cycles: differences and competition, Geochim. Cosmochim. Acta 288 (2020) 51–67, https://doi.org/10.1016/j.gca.2020.08.007.

[250] Z. Yin, L. Ye, W. Zhong, C. Jing, Thiolation of trimethylantimony: identification and structural characterization, J. Hazard. Mater. 423 (2022) 127259, https://doi.org/10.1016/j.jhazmat.2021.127259.

[251] X. Yang, Q. Peng, L. Liu, W. Tan, G. Qiu, C. Liu, et al., Synergistic adsorption of Cd(II) and As(V) on birnessite under electrochemical control, Chemosphere 247 (2020) 125822, https://doi.org/10.1016/j.chemosphere.2020.125822.

[252] H. Yin, H. Li, Y. Wang, M. Ginder-Vogel, G. Qiu, X. Feng, et al., Effects of Co and Ni co-doping on the structure and reactivity of hexagonal birnessite, Chem. Geol. 381 (2014) 10–20, https://doi.org/10.1016/j.chemgeo.2014.05.017.

[253] H. Yin, F. Liu, X. Feng, M. Liu, W. Tan, G. Qiu, Co^{2+}-exchange mechanism of birnessite and its application for the removal of Pb^{2+} and As(III), J. Hazard. Mater. 196 (2011) 318–326, https://doi.org/10.1016/j.jhazmat.2011.09.027.

[254] M. Polverejan, J.C. Villegas, S.L. Suib, Higher valency ion substitution into the manganese oxide framework, J. Am. Chem. Soc. 126 (2004) 7774–7775, https://doi.org/10.1021/ja048985y.
[255] S. Zhao, Y.A. González-Valle, E.J. Elzinga, E.M. Saad, Y. Tang, Effect of Zn(II) coprecipitation on Mn(II)-induced reductive transformation of birnessite, Chem. Geol. 492 (2018) 12–19, https://doi.org/10.1016/j.chemgeo.2018.05.031.
[256] Q. Zheng, J. Hou, W. Hartley, L. Ren, M. Wang, S. Tu, et al., As(III) adsorption on Fe-Mn binary oxides: are Fe and Mn oxides synergistic or antagonistic for arsenic removal? Chem. Eng. J. 389 (2020) 124470 https://doi.org/10.1016/j.cej.2020.124470.
[257] K. Sasaki, M. Matsuda, T. Urata, T. Hirajima, H. Konn, Sorption of Co ions on biogenic Mn oxides produced by a Mn-oxidizing fungus, *Paraconiothyrium* sp.-like strain, Adv. Mater. Res. 20–21 (2007) 607–610, https://doi.org/10.4028/www.scientific.net/AMR.20-21.607.
[258] X. Zhao, Z. Xie, P. Li, M. Chen, Z. Zhong, A newly isolated indigenous metal-reducing bacterium induced Fe and Mn oxides synergy for enhanced in situ As(III/V) immobilization in groundwater, J. Hydrol. 608 (2022) 127635, https://doi.org/10.1016/j.jhydrol.2022.127635.
[259] H. Cui, X. Feng, F. Liu, W. Tan, J. He, Factors governing formation of todorokite at atmospheric pressure, Sci. China Ser. D-Earth Sci. 48 (2005) 1678–1689, https://doi.org/10.1360/01yd0550.
[260] Y. Cruz-Hernández, M. Villalobos, M.A. Marcus, T. Pi-Puig, R. Zanella, N. Martínez-Villegas, Tl(I) sorption behavior on birnessite and its implications for mineral structural changes, Geochim. Cosmochim. Acta 248 (2019) 356–369, https://doi.org/10.1016/j.gca.2019.01.020.
[261] D. Wei, J. Liu, Z. Luo, X. Xie, Insight into the reactions of antimonite with manganese oxides: synergistic effects of Mn(III) and oxygen vacancies, Water Res. 232 (2023) 119681, https://doi.org/10.1016/j.watres.2023.119681.
[262] N. Karimian, K. Hockmann, B. Planer-Friedrich, S.G. Johnston, E.D. Burton, Antimonate controls Manganese(II)-induced transformation of birnessite at a circumneutral pH, Environ. Sci. Technol. 55 (2021) 9854–9863, https://doi.org/10.1021/acs.est.1c00916.
[263] N. Karimian, S.G. Johnston, E.D. Burton, Reductive transformation of birnessite and the mobility of co-associated antimony, J. Hazard. Mater. 404 (2021) 124227, https://doi.org/10.1016/j.jhazmat.2020.124227.
[264] W. Xu, H. Wang, R. Liu, X. Zhao, J. Qu, The mechanism of antimony(III) removal and its reactions on the surfaces of Fe–Mn Binary Oxide, J. Colloid Interface Sci. 363 (2011) 320–326, https://doi.org/10.1016/j.jcis.2011.07.026.
[265] H. Lu, W. Zhang, L. Tao, F. Liu, J. Zhang, Enhanced removal of antimony by acid birnessite with doped iron ions: companied by the structural transformation, Chemosphere 226 (2019) 834–840, https://doi.org/10.1016/j.chemosphere.2019.03.194.